

Catchment-scale LiDAR-based SedNetNZ modelling of erosion and suspended sediment loads in Waikato CEM catchments



Prepared by	Simon Vale, Hugh Smith, Maksym Polyakov (Bioeconomy Science Institute)
For	Waikato Regional Council Private Bag 3038 Waikato Mail Centre HAMILTON 3240
Publication date	October 2025
Document ID	31722281

	Name	Date
Peer Reviewer	Andrew Hughes (NIWA)	March 2025
Approving Manager	Mike Scarsbrook Tracey May	June 2025 June 2025

Disclaimer

This technical report has been prepared for the use of Waikato Regional Council as a reference document and as such does not constitute Council's policy.

Council requests that if excerpts or inferences are drawn from this document for further use by individuals or organisations, due care should be taken to ensure that the appropriate context has been preserved, and is accurately reflected and referenced in any subsequent spoken or written communication.

While Waikato Regional Council has exercised all reasonable skill and care in controlling the contents of this report, Council accepts no liability in contract, tort or otherwise, for any loss, damage, injury or expense (whether direct, indirect or consequential) arising out of the provision of this information or its use by you or any other party.

Doc # 31722281 Page i



Catchment-scale LiDAR-based SedNetNZ modelling of erosion and suspended sediment loads in Waikato CEM catchments

October 2025

Simon Vale, Hugh Smith, Maksym Polyakov

Bioeconomy Science Institute, Manaaki Whenua – Landcare Research Group

Contract Report Registration Number: 2526-0045

Prepared for: Waikato Regional Council

Disclaimer

This report has been prepared by the New Zealand Institute for Bioeconomy Science Ltd for Waikato Regional Council. If used by other parties, no warranty or representation is given as to its accuracy and no liability is accepted for loss or damage arising directly or indirectly from reliance on the information in it.

Reviewed by:

Andrew Neverman
Senior Researcher - Geomorphology / Erosion and
Sediment Processes and Research Priority Area Leader
Bioeconomy Science Institute, Manaaki Whenua – Landcare
Research group

Approved for release by:

Sam Carrick
Portfolio Leader – Land Resources and Climate Change
Bioeconomy Science Institute, Manaaki Whenua –
Landcare Research group

Contents

Sumi	mary.		III
1	Intro	oduction	1
	1.1	Objectives	1
2	Back	ground	1
	2.1	SedNetNZ	1
	2.2	LiDAR-based SedNetNZ	3
3	Meth	hods	3
	3.1	LiDAR pre-processing for erosion modelling	3
	3.2	LiDAR-based SedNetNZ model description	7
	3.3	Model simulations	17
	3.4	Reductions for NPS-FM visual clarity attribute bands	22
4	Resu	ılts	29
	4.1	LiDAR-based SedNetNZ erosion and sediment load model for the CEM catchments	29
	4.2	Sediment load reductions required to meet NPS-FM visual clarity attribute bands	44
	4.3	Model evaluation and limitations	56
5	Cond	clusions	63
6	Ackr	nowledgements	64
7	Refe	rences	65
Anne	ndiv	1	73

Summary

Project and client

- Waikato Regional Council (WRC) contracted Manaaki Whenua Landcare Research (MWLR) to model erosion and suspended sediment loads in four catchments from the Catchment Environmental Monitoring (CEM) programme using the newly developed LiDAR-based version of the SedNetNZ model. The CEM catchments include the Kaniwhaniwha (100 km²), Karapiro (67 km²), Matahuru (110 km²), and the Moakurarua (200 km²).
- The project involved generating a new digital stream network from a 5 m digital elevation model (DEM) for each catchment and developing a high-resolution landslide susceptibility model to predict shallow landslide erosion. These layers were used in SedNetNZ to model contemporary suspended sediment loads for CEM catchments as well as future erosion mitigation scenarios.
- The project also assessed the load reductions required to meet National Policy Statement for Freshwater Management (NPS-FM 2020) targets.

Note: An economic analysis was included in the project, which evaluated the cost-effectiveness of erosion mitigation works in achieving visual water clarity targets defined by the National Objectives Framework (NOF) for suspended fine sediment. This analysis was not included in this abridged version of the report for release.

Objectives

The project had the following objectives:

- update the contemporary suspended sediment loads for CEM catchments using the LiDAR-based version of the SedNetNZ model
- model future erosion mitigation scenarios, including bush retirement/afforestation, space-planted trees, and riparian retirement under two implementation scenarios
- assess load reductions required to meet NPS-FM (2020) attribute bands and the national bottom line (NBL) for suspended fine sediment at monitoring sites.

Methods

LiDAR-based SedNetNZ model description

- A digital stream network was generated for each catchment from a sink-filled 5 m DEM using a flow direction and accumulation algorithm with a 5 ha channel initiation threshold.
- The SedNetNZ sub-models were adapted to incorporate LiDAR-derived DEMs, including:
 - integration of a high-resolution landslide susceptibility layer into the shallow landslide erosion sub-model
 - full implementation of the Revised Universal Soil Loss Equation (RUSLE) using LiDAR-derived topographic inputs in the surface erosion sub-model
 - implementation of a data-driven riverbank erosion sub-model.
 - redefining overbank sediment deposition areas using the LiDAR-based 5 m DEM.

Erosion mitigation scenarios

- The contemporary baseline uses recent land cover (LCDBv5, 2018), soil conservation works, and estimated riparian fencing based on the CEM riparian surveys. The surface erosion submodel now incorporates stock density data to represent the effect of livestock treading on soil erodibility.
- Two future erosion mitigation scenarios were modelled using a 'ranked-watershed' approach applied within each catchment, targeting 20% to 100% of pastoral land based on slope thresholds.
 - *Mitigation scenario 1 (M1*) included retirement and afforestation of pastoral land on slopes \geq 35° and space-planted trees on slopes \geq 26° and < 35°.
 - *Mitigation scenario 2 (M2)* included retirement and afforestation of pastoral land on slopes \geq 30° and space-planted trees on slopes \geq 26° and < 30°.
 - Riparian stock-exclusion fencing was applied to both scenarios based on Regional Plan Change 1 rules (Waikato Regional Council 2020).¹

Reductions for NPS-FM visual clarity attribute bands

• Proportional and absolute load reductions required to meet NPS-FM 2020 attribute bands and the NBL for the state of the environment (SOE) monitoring sites for each CEM catchment were assessed for the contemporary and future mitigation scenarios.

Results

CEM catchment SedNetNZ erosion and sediment loads

- The LiDAR-based SedNetNZ model estimated net suspended sediment load delivered to the catchment outlet amounted to 33.4 kt yr⁻¹, 14.4 kt yr⁻¹, 13.2 kt yr⁻¹, and 6.6 kt yr⁻¹ for Moakurarua, Matahuru, Kaniwhaniwha, and Karapiro, respectively.
- Over a multi-decadal timescale, shallow landslides contribute an estimated 81% of the suspended sediment load in Matahuru, 56% in Kaniwhaniwha, 54% in Karapiro, and 42% in Moakurarua. Surface erosion accounts for 14%–46% across the CEM catchments, while riverbank erosion contributes 6%–13%.

Erosion mitigation scenario erosion and sediment loads

- Under the M1 scenario, total erosion load decreases by 8%–14% relative to the contemporary baseline with 20% implementation across the CEM catchments. A slightly larger reduction of 9%–16% is observed under the M2 scenario. Full implementation results in reductions of 21%–41% under M1 and 23%–45% under M2.
- The Matahuru catchment shows the largest proportional reductions, with total erosion under full implementation decreasing by 41% and 45% under the M1 and M2 scenarios, respectively. The Kaniwhaniwha shows reductions of 24% and 26% and Moakurarua shows reductions of 24% and 28% under M1 and M2, respectively. The Karapiro has the smallest reductions of 21% and 23% under M1 and M2, respectively. In terms of absolute reductions,

¹ See: Waikato Regional Council (WRC) 2020. Proposed Waikato Regional Plan Change 1: Waikato and Waipā River Catchments (Decisions Version). Waikato Regional Council Policy Series 2020/02. www.waikatoregion.govt.nz. (accessed September 2024).

- Moakurarua has the largest total load reductions of 8.5 and 9.6 kt yr⁻¹, under M1 and M2, respectively.
- Under individual erosion mitigation scenarios, Matahuru has the largest reductions from afforestation and bush retirement (16% under M1, and 32% under M2), followed by Moakurarua (12% under M1 and 20% under M2), and Kaniwhaniwha (11% under M1 and 18% under M2). Karapiro shows the smallest reductions (7% under M1 and 14% under M2).
- Space-planted trees also provide substantial sediment load reductions, particularly in Matahuru (24% under M1 and 12% under M2) and Kaniwhaniwha (17% under M1 and 12% under M2). Moakurarua (12% under M1 and 7% under M2) and Karapiro (12% under M1 and 7% under M2) show more moderate reductions.
- Riparian stock-exclusion fencing has the smallest proportional sediment load reductions, with the highest reductions occurring in Kaniwhaniwha (7%), followed by Moakurarua (5%), Matahuru (4%) and Karapiro (4%).

Reductions in sediment loads for NPS-FM visual clarity attribute bands

- All SOE sites for the contemporary baseline require reductions to achieve the NBL, with required reductions of 62% for Matahuru, 55% for Kaniwhaniwha, 51% for Karapiro, and 36% for Moakurarua. Achieving the B and A attribute bands requires reductions ranging from 47%–72% and 56%–78%, respectively.
- After applying the M1 and M2 scenarios, further load reductions are required to achieve the NBL. Under full implementation, achieving the NBL still requires reductions of 32%–36% for Matahuru, 37%–39% for Kaniwhaniwha, 38%–40% for Karapiro, and 12%–15% for Moakurarua. At full implementation, neither M1 nor M2 achieves the NBL at any of the SOE sites.
- A similar pattern is observed for B and A attribute bands. Achieving attribute band A requires further reductions of 61%–63% for Matahuru, 57%–58% for Kaniwhaniwha, 58%–59% for Karapiro, and 39%–42% for Moakurarua at full implementation.

Conclusions

Conclusion

- The LiDAR-based SedNetNZ model estimated net suspended sediment load delivered to the CEM catchment outlets ranged from 6.6 kt yr⁻¹ to 33.4 kt yr⁻¹. Shallow landslides are the dominant sediment source, followed by surface and riverbank erosion.
- Erosion mitigation scenarios showed that implementing erosion control works could reduce total sediment loads by 21%–45% under M1, and 23%–45% under M2. Despite these reductions, none of the mitigation scenarios achieved the NPS-FM (2020) NBL at any of the SOE sites. At full implementation of M1 and M2, further reductions between 12% and 40% would still be needed to meet the NBL across the CEM catchments.
- Modelled suspended sediment loads are generally consistent with suspended sediment concentration (SSC)- discharge (Q) rating curve estimates of load from the river monitoring sites, as well as with previous region-wide SedNetNZ modelling (Vale & Smith 2024)², albeit

² See: Vale S, Smith H 2024. Application of SedNetNZ in the Waikato region to support NPS-FM 2020 implementation. Manaaki Whenua – Landcare Research Contract Report LC4432, prepared for Waikato Regional Council.

slightly lower; except for Kaniwhaniwha, where the load is marginally higher. These differences reflect variations in modelled soil conservation works, such as riparian fencing, and changes in erosion process representation within the LiDAR-based erosion process submodels.

- Compared to previous region-wide SedNetNZ modelling, there is a general decrease in the relative contribution of shallow landslides, accompanied by an increase in surface and riverbank erosion across all CEM catchments. Absolute sediment loads from shallow landslides remain similar in Kaniwhaniwha and Matahuru, with larger reductions in Karapiro and Moakurarua using the higher-resolution data. Surface erosion contributions have approximately doubled in Kaniwhaniwha, Karapiro, and Matahuru. Riverbank erosion loads have approximately doubled across all CEM catchments, largely due to an increase in the length of the modelled LiDAR DEM-derived digital stream network.
- The benefits of using higher resolution LiDAR-derived DEMs in erosion and sediment load modelling include: a) improved model parameterisation and predictive performance due to the more accurate representation of topography (e.g. slope angles, curvature); b) better representation of the stream network (e.g. channel sinuosity, channel slope, bank height); c) the ability to provide higher resolution raster layers for selected erosion processes, namely shallow landslide, and surface erosion.

1 Introduction

Waikato Regional Council (WRC) contracted Manaaki Whenua – Landcare Research to model erosion and suspended sediment loads using the newly developed LiDAR-based version of the SedNetNZ model in four catchments from the Catchment Environmental Monitoring (CEM) programme in the Waikato region. The CEM catchments include the Kaniwhaniwha (107 km²), Karapiro (84 km²), Matahuru (114 km²), and the Moakurarua (228 km²) (Figure 1).

1.1 Objectives

The project had the following objectives:

- update the contemporary suspended sediment loads for CEM catchments using the LiDAR-based version of the SedNetNZ model
- model future erosion mitigation scenarios, including bush retirement/afforestation, spaceplanted trees, and riparian retirement under two implementation scenarios
- assess load reductions required to meet National Policy Statement for Freshwater Management (NPS-FM 2020) attribute bands and the national bottom line (NBL) for suspended fine sediment at monitoring sites

Note: An economic analysis was included in the project, which evaluated the cost-effectiveness of erosion mitigation works in achieving visual water clarity targets defined by the National Objectives Framework (NOF) for suspended fine sediment. This analysis was not included in this abridged version of the report for release.

2 Background

2.1 SedNetNZ

The SedNetNZ sediment budget model represents the range of erosion processes that occur in New Zealand. These include shallow landslide, earthflow, gully, surface erosion (sheet/rill), and riverbank erosion (Dymond et al. 2016; Smith, Spiekermann et al. 2019). In the non-LiDAR based version of SedNetNZ, hillslope erosion processes are computed using the national 15 m digital elevation model (DEM) derived from contour data. Bank erosion is estimated for each segment of the digital stream network developed for the River Environment Classification v2 (REC2). The sediment loads from these processes are combined and routed through the digital stream network while accounting for losses due to floodplain deposition and trapping in lakes to estimate the mean annual suspended sediment load for each REC2 subwatershed (area draining to a segment in the digital steam network) within the catchment.

SedNetNZ modelling for the Waikato region (Vale & Smith 2024) was recently completed using the latest non-LiDAR based version of the SedNetNZ model to provide consistent, region-wide model outputs to replace previous SedNetNZ modelling completed between 2013 and 2017 (Palmer et al. 2013, 2015; Betts, Spiekermann et al. 2017). The latest non-LiDAR version of the model included significant updates compared to the version previously applied in the region. These improvements

included an enhanced bank erosion model that incorporated riparian woody vegetation, channel sinuosity, and bank erodibility (Smith et al. 2019, 2020); improved representation of surface runoff-contributing areas and spatially variable soil erodibility for surface erosion (Neverman et al. 2021); integration of lake sediment trapping in stream network routing (Neverman et al. 2021); and refined estimation of floodplain deposition to better reflect upstream sediment loads (Vale et al. 2021).

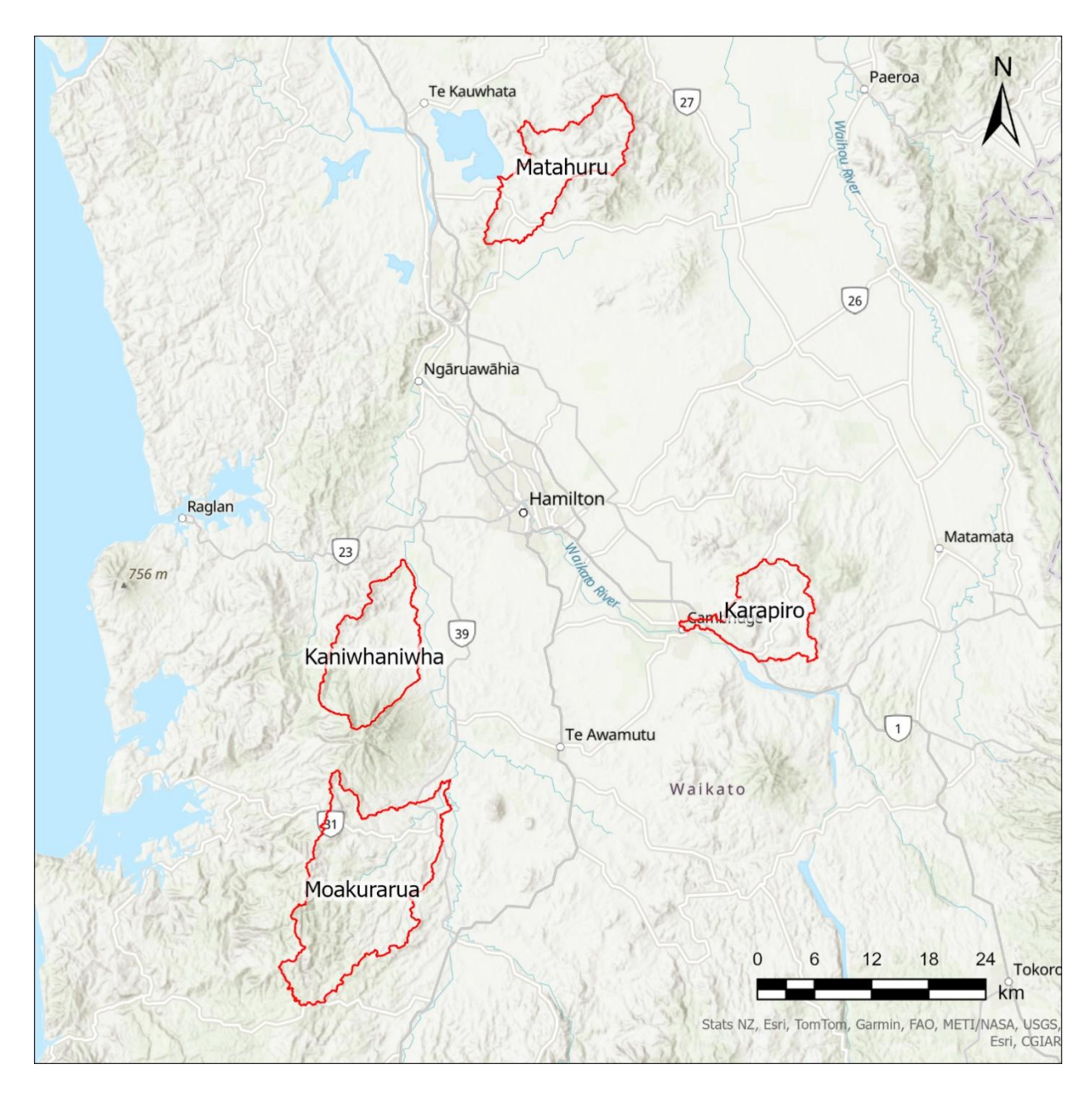


Figure 1. Current CEM catchments for the LiDAR-based SedNetNZ modelling: Kaniwhaniwha, Karapiro, Matahuru, and the Moakurarua.

The SedNetNZ modelling by Vale & Smith (2024) for the Waikato region represented recent land cover and erosion mitigations, as well as a range of future erosion mitigation and climate change scenarios. Additionally, backward-looking scenarios were developed to represent past land cover and riparian fencing based on the 2002, 2007, 2012, and 2017 regional riparian surveys. Sediment load reductions required to meet NPS-FM 2020 (Ministry for the Environment 2022) attribute

bands and the national bottom line (NBL) for suspended fine sediment (visual clarity) were also assessed for the baseline and future mitigation scenarios, with and without the effects of climate change.

2.2 LiDAR-based SedNetNZ

The LiDAR-based version of SedNetNZ includes changes to the shallow landslide, riverbank, and surface erosion sub-models, as well as in the representation of sediment entering floodplain storage (Smith et al. 2024). The earthflow and gully erosion sub-models have not changed.

Benefits of using higher resolution LiDAR-derived DEMs in erosion and sediment load modelling may include: a) improved model parameterisation and predictive performance due to the more accurate representation of topography (e.g. slope angle, curvature); b) better representation of the stream network (e.g. channel sinuosity, channel slope, bank height); c) the ability to provide higher resolution raster layers for selected erosion processes (Smith et al. 2024).

Specific changes in the LiDAR-based SedNetNZ compared to the current non-LiDAR SedNetNZ model include:

- 1 replacing the national 15 m DEM based on contours with a LiDAR-derived 5 m DEM for use in erosion process modelling.
- 2 generating new digital stream network and subwatershed layers using the LiDAR-derived 5 m DEM.
- 3 upgrading the rainfall-induced shallow landslide erosion sub-model based on high-resolution, data-driven landslide susceptibility modelling to provide improved assessment of the spatial patterns in shallow landslide erosion based on the underpinning susceptibility model.
- 4 upgrading the riverbank erosion sub-model based on data-driven modelling that draws on an expanded dataset of channel planform change (increased from 77 to over 800 km of mapped channels) for use in model training.
- upgrading the surface erosion sub-model with the Revised Universal Soil Loss Equation (RUSLE) based on the LiDAR-derived DEM with rainfall erosivity computed from interpolated mean annual rainfall grids, while slope and runoff-contributing areas are computed from the LiDAR-derived DEM.
- replacing the previous representation of floodplains based on New Zealand Land Resource Inventory (NZLRI) mapping at 1:63,360 scale. The extent of floodplain alongside channels where flows may go overbank and deposit sediment is now determined from the LiDAR-based 5 m DEM.

3 Methods

3.1 LiDAR pre-processing for erosion modelling

The 2021 LiDAR dataset for the Waikato region was obtained from LINZ in July 2024 (Land Information New Zealand 2021), clipped to the four CEM catchment extents and resampled to a 5 m DEM for use in erosion modelling.

3.1.1 Digital stream network

Digital stream network and subwatershed layers were produced for use in the erosion and sediment load modelling in each CEM catchment. The network was generated from the sink-filled DEM using a D8 flow direction and accumulation algorithm and a 5 ha channel initiation threshold. The D8 algorithm models the flow direction from a cell to its steepest downslope neighbour. Each segment within the digital network for each CEM catchment has a corresponding subwatershed draining to the segment.

The digital stream networks were used to apply the bank erosion sub-model. Therefore, the networks needed to approximate the physical extent of stream channels where fluvial scour may occur as flow is concentrated within banks (i.e. excludes zero order, un-channelised drainage lines). We compared the 5 ha network with networks derived using 1 ha and 10 ha initiation thresholds using high-resolution aerial imagery and hillshade layers in each catchment to identify channels. While underestimation and overestimation of the channel extent occurs in places, the 5 ha network was considered to provide the best overall approximation of the physical channel network. A potential LiDAR-based approach to detecting channel head locations was not applied because of the size of incipient channels. These are likely to sit below the minimum vertical accuracy (e.g. non-vegetated areas ≤ 0.2 m at a 95% confidence interval) for the LiDAR point cloud (Land Information New Zealand 2021), while vertical accuracy will be further reduced for areas under woody vegetation cover.

We manually refined the 5 ha digital network in each catchment to correct major errors in channel planform arising from the presence of infrastructure (e.g. bridges, culverts etc.) that prevent the digital network from following the natural drainage line. We also revised parts of the network that occurred in very low-relief areas with extensive modified drainage. In these cases, the algorithm was unable to produce a representative network, so we manually digitised the network from aerial imagery.

Differences in channel network length between the LiDAR DEM-derived network and the REC2 digital network reflect both differences in channel initiation thresholds and channel sinuosity (Table 1). The LiDAR DEM-derived networks provide a better representation of the sinuous planform of channels compared to the REC2 network (Figure 2).

Table 1. Comparison of total refined length of the stream network based on REC2 and LiDAR-derived 5 m DEM for each CEM catchment

CEM catchment	Digital stream network length (km)					
	REC2 LiDAR 5 m DEM 5 ha					
Kaniwhaniwha	210	439				
Karapiro	144	316				
Matahuru	172	412				
Moakurarua	363	762				

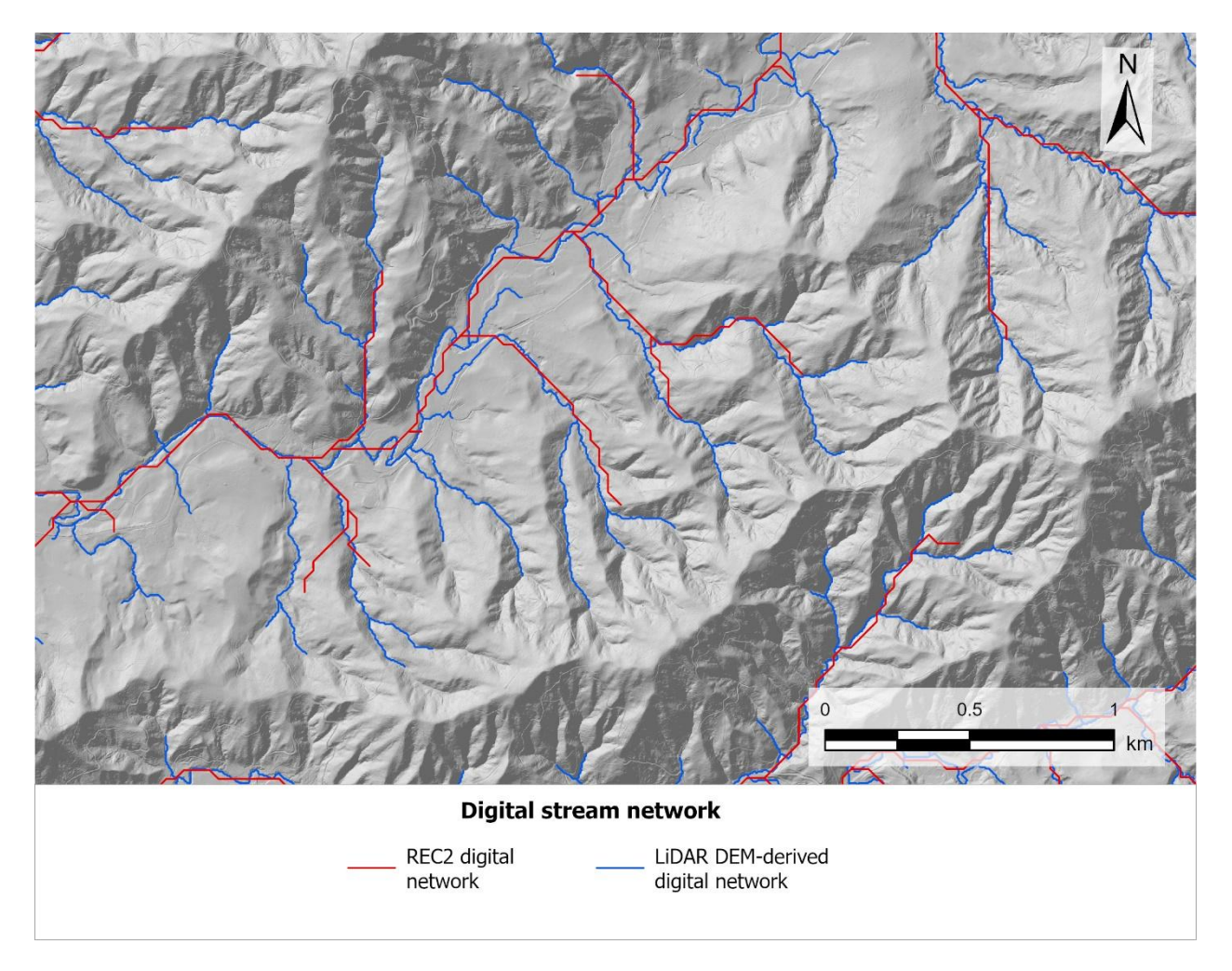


Figure 2. Example of the new LiDAR DEM-derived digital network (blue) compared to the previous REC2 digital network (red), showing improved planform accuracy and stream representation.

3.1.2 Shallow landslide susceptibility

The LiDAR-based version of SedNetNZ integrates high-resolution landslide susceptibility with the shallow landslide erosion sub-model to estimate landslide-derived sediment loads (described in Section 3.2.1). This development requires spatial prediction of shallow landslide susceptibility using a statistical susceptibility model (Smith et al. 2024). In this section, we describe the approach to modelling rainfall-induced shallow landslide susceptibility using the LiDAR-derived DEMs in the four CEM catchments. Landslide susceptibility modelling involved: a) assembling a data set

comprising landslides located in areas with LiDAR coverage; b) applying a logistic regression model and evaluating model performance; c) predicting landslide susceptibility at 5 m resolution in each catchment.

The data set available for susceptibility modelling in the present study comprises shallow landslides (over n = 123,000) assembled from mapping areas in the Hawke's Bay, Gisborne, Greater Wellington, and Waikato regions that overlap with existing LiDAR coverages (Table 2). This combined data set exceeds that previously used in Smith et al. (2024) with the addition of landslide data from the Waikato region. Non-landslide locations were randomly selected from within these landslide mapping areas to produce a balanced sample comprising equal numbers of landslide and non-landslide points for statistical modelling (Smith et al. 2021).

Binary logistic regression (BLR) was used to classify landslide and non-landslide locations. This type of regression requires spatial data corresponding to landslide/non-landslide locations for variables that may influence susceptibility. The analysis draws on spatial data sets for elevation (5 m LiDAR-derived DEM), land cover (LCDB) and rock type (NZ Land Resources Inventory; Newsome et al. 2008). Slope angle (continuous variable), aspect (categorical variable with 8 classes), profile (categorical: convex, concave, planar) and planform curvature (categorical: convergent, divergent, planar) were also derived from the DEM. These input variables were selected for use in statistical modelling because: a) there is a potential physical basis for how each variable may influence landslide susceptibility (Smith et al. 2021); b) model inputs can be derived for all areas.

Table 2. Summary information for the landslide mapping areas with LiDAR coverage contributing data to the shallow landslide data set used for susceptibility modelling in the CEM catchments

Location	Study area (km²)	Period	Number of landslides	Imagery sources (resolution)	Data source
Southern Hawke's Bay	175	Event (2011)	27,170	Orthorectified aerial photography and Worldview-2 (0.4 m)	Smith et al. (2021)
Northern Hawke's Bay and Gisborne	3,162	Multi-event (2022)	45,879	Orthorectified aerial photography (0.3 m) and Pleiades (0.5 m)	Betts et al. (2023)
Wairarapa, Greater Wellington	843	Multi-event (2005-10)	43,069	Orthorectified aerial photography (0.4 m)	Spiekermann et al. (2021)
Wairamarama, Waikato	178	Event (2017)	7,704	Pleiades-1A and GeoEye-1 (0.5 m)	Smith et al. (2021)

Binary logistic regression has been widely applied internationally for landslide susceptibility analysis (Reichenback et al. 2018). This regression is a type of generalised linear model (GLM) that uses a logistic function with a binary dependent variable (landslide presence/absence). It relates the probability (P) of landslide presence (Y = 1) to the spatial explanatory variables ($x_1, x_2,...x_n$) where β_0 , $\beta_1, \beta_2...\beta_n$ are fitted constants (Equation 1):

$$P(Y=1) = \frac{1}{1 + e^{-(\beta_0 + \beta_1 x_1 + \beta_2 x_2 \dots \beta_n x_n)}}$$
(1)

Model predictive performance was assessed using k-fold cross-validation. The data set comprising landslide and non-landslide locations was randomly shuffled and then split into k = 5 folds, where k - 1 folds were used for model training and each remaining fold (20% of the data) was used once for testing. Sensitivity to the location of non-landslide points was also tested by repeating the randomised placement of absence points five times. The procedure was repeated to produce a total of 100 data partitions for model fitting and testing.

Model classification performance (i.e. landslide versus non-landslide) was evaluated using receiver operating characteristic (ROC) curves and calculation of the area under curve (AUC) based on the 100 iterations. ROC curves and AUC values are widely used in the landside susceptibility literature to assess model performance (Reichenbach et al. 2018). The ROC curves plot the true positive rate $(TPR = \frac{TP}{TP + FN})$ versus the false positive rate $(FPR = \frac{FP}{TN + FP})$ to give an indication of sensitivity (probability of detection) versus 1 – specificity (where specificity refers to the true negative rate) (Conoscenti et al. 2016). An AUC value of 0.5 corresponds to performance no better than a random guess, while a value of 1 indicates perfect classification. Model performance is generally considered 'fair' above 0.7, 'good' between 0.8-0.9, and 'excellent' above 0.9 (Carter et al. 2016). In the present version, the BLR model achieved a median AUC of 0.9 in cross-validation.

The fitted BLR model was used to produce spatial predictions of shallow landslide susceptibility at 5 m resolution. This involved applying the model in each catchment with the set of explanatory variables as raster inputs to predict shallow landslide susceptibility, which is expressed as a spatial probability (range 0-1). These landslide susceptibility predictions were used in the shallow landslide erosion sub-model that forms part of the LiDAR-based SedNetNZ (see Section 3.2.1).

3.2 LiDAR-based SedNetNZ model description

SedNetNZ computes a mean annual suspended sediment budget for the subwatershed draining to each segment in the LiDAR DEM-derived digital stream network. Each sediment budget comprises erosion process (i.e. surface, shallow landslide, gully, earthflow, and riverbank) sediment loads delivered to the stream segment minus any sediment entering floodplain storage (see Fig. 2 in Dymond et al. 2016). The resulting net suspended sediment load is then routed to the next downstream segment and through the network to the catchment outlet, while accounting for deposition in lakes.

Predictions of mean annual surface and shallow landslide erosion using the LiDAR DEM-based submodels were produced on a 5 m grid, while bank erosion was estimated for each stream segment in the digital network. Net suspended sediment loads and sediment yields are computed for each subwatershed draining to a digital stream segment for each CEM catchment.

3.2.1 Shallow landslide sub-model

Shallow landslides are considered the most common form of erosion in New Zealand hill country (Basher 2013; Eyles 1983; Phillips et al. 2021). Shallow landslides are typically < 2 m deep and individual source areas (scars) are generally small (median size 50–100 m²) (Betts, Basher et al. 2017; Smith et al. 2021). Landslide-triggering storm events occur episodically and thus the contribution of shallow landslides to suspended sediment loads will exhibit significant inter-annual variation. For this reason, SedNetNZ averages across a multi-decadal period to estimate the longer-

term contribution of shallow landslides to mean annual suspended sediment loads rather than attempting to estimate the contribution for any given year.

In previous applications of SedNetNZ, the mass of soil eroded by shallow landslides and delivered to the stream network per square kilometre per year (*EL*) was estimated by:

$$EL = \rho \, SDR \, d_l f(s) \tag{2}$$

where ρ is the bulk density of soil (t m⁻³), SDR is the sediment delivery ratio, d_l is the mean depth of landslide failure (m), and f(s) is the expected area of landslide scars per square kilometre per year at slope angle s (m² km⁻² yr⁻¹) for terrain under grass cover.

In the non-LiDAR based version of the model, shallow landslide erosion was estimated for those erosion terrains³ (Dymond et al. 2010) identified as being susceptible to landslide erosion; ρ is set to 1.5 t m⁻³ (Dymond et al. 2016); SDR values are typically 0.5 in hill country and 0.1 in hard rock mountain areas (Dymond et al. 2016); d_l is set to 1 m (Page et al. 1994; Reid & Page 2002; Betts, Basher, et al. 2017; Phillips et al. 2021); and f(s) is determined from previous calibration of SedNetNZ using multi-temporal landslide mapping data from historical aerial imagery spanning approximately 70 years for study areas in the Manawatū catchment (Dymond et al. 2016; Betts, Basher et al. 2017). The difference in SDR between hill country and hard rock mountain areas reflects the tendency for landslides in mountains to contain a larger proportion of rock (Dymond et al. 2016).

Permanent woody cover is estimated to reduce shallow landslide erosion by 90% compared with pasture (Basher 2013; Dymond et al. 2016; Phillips et al. 2020; Smith et al. 2023), while an estimated 80% reduction was applied for exotic plantations over multiple rotations (first applied in Vale et al. 2021). The lower reduction estimated for plantation versus permanent forest recognises the effectiveness of forest cover for reducing shallow landslides (Marden 2012; Smith et al. 2023) for much of the rotation while acknowledging the period spanning several years between harvest and canopy closure of the replanted crop during which there is an increase in susceptibility to shallow landslide erosion (Phillips et al. 2018, 2024).

Upgraded shallow landslide sub-model

In the LiDAR-based version of SedNetNZ, the spatial predictions of shallow landslide susceptibility (described in Section 3.1.2) are used as an input to the shallow landslide erosion sub-model. This new approach replaces the erosion terrains layer with higher resolution (5 m) information based on statistical landslide susceptibility modelling.

The upgraded shallow landslide erosion sub-model draws on the same multi-temporal landslide mapping data from study areas in the Manawatū catchment (Dymond et al. 2016). However, we now relate the landslide-eroded area to slope (i.e. f(s)) using photogrammetrically derived 2 m DEMs (in the absence of LiDAR) from the Manawatū study areas that span soft and hard rock areas

³ An erosion terrain is a land type with a distinct combination of erosion processes and rates leading to characteristic sediment generation and yields. Erosion terrains were derived from New Zealand Land Resource Inventory data and are based on combinations of rock type/parent material, topography, rainfall, and erosion process type and severity.

(Betts, Basher et al. 2017). These DEMs were resampled to 5 m for consistency with the Waikato 5 m DEM. These revised landslide-eroded area versus slope relationships (Figure 3b) replace the single landslide-slope relationship originally based on the national 15 m DEM (Dymond et al. 2016; (Figure 3a). We derived the soft rock landslide-slope relationship using data from landslide mapping of hill country areas under mostly grass cover (Betts, Basher et al. 2017). The hard rock relationship was based on landslide mapping data for greywacke ranges under woody vegetation (Fuller et al. 2016). Therefore, the lower landslide eroded area per 1° slope bin for hard rock terrain in (Figure 3b reflects the influence of both woody cover and rock type on landslide erosion.

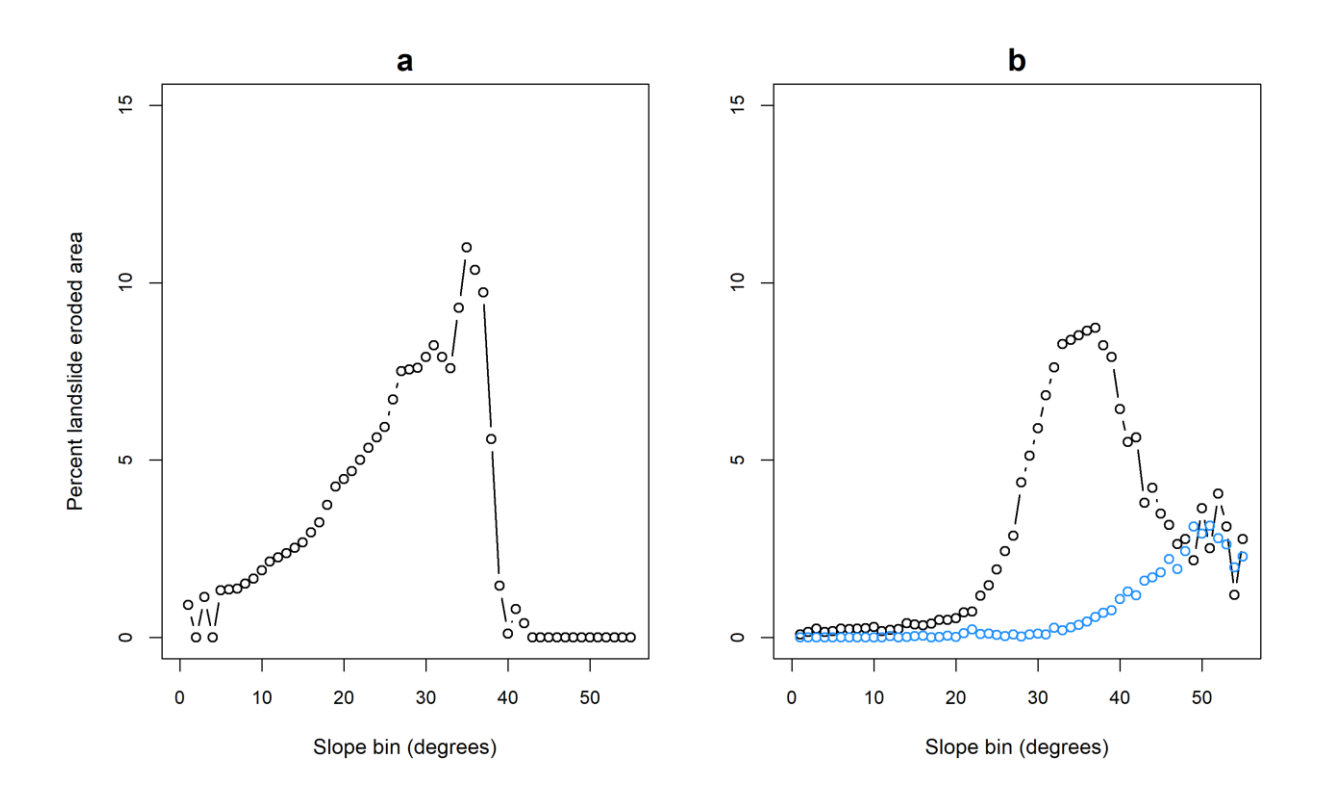


Figure 3. Plots of landslide eroded area (expressed as a percentage of each slope bin) per 1-degree slope bin for: a) national 15 m DEM (previous SedNetNZ model; Dymond et al. 2016); b) 5 m DEM for soft rock under grass (black circles) and hard rock under woody vegetation (blue circles) terrain based on multitemporal polygon mapping (70-year interval) of shallow landslide erosion in the Manawatū catchment. (Source: Reproduced from Smith et al. 2024.)

The sediment load from shallow landslide erosion is distributed across the landscape based on the spatial probabilities from the modelled landslide susceptibility. The 2018 land cover from LCDB v5.0 was reclassified into woody cover on hard rock areas and grass cover on non-hard rock terrain. This reclassified cover layer is used to predict landslide susceptibility, and the resulting susceptibility layer forms the basis for applying the landslide-slope relationships across the catchments. This was achieved using a 'percentile matching' approach whereby percentiles derived from the pixel-based spatial probabilities from the susceptibility layer were separately matched to the equivalent slope percentiles in 1-degree increments (bins) for the woody cover on hard rock and grass on non-hard rock domains (Smith et al. 2024). This enabled the landslide-eroded area per 1-degree slope bin (i.e. f(s)) to be distributed spatially at 5 m resolution for each domain.

Given the difference in the reference vegetation cover (grass versus woody) for the rock type-based landslide calibration data (Figure 3), the reduction in landslide erosion by 80% (exotic plantation) or

90% (permanent woody cover) was only applied on non-hard rock terrain where woody vegetation was present. In contrast, landslide erosion was increased by an inverse proportion (i.e. 10-fold) in those hard rock areas under non-woody vegetation to represent the higher rates of landslide erosion that generally occur in the absence of woody cover.

To prevent small amounts of landslide erosion from occurring on very low slope land, a slope threshold of 6 degrees was applied below which landslide erosion was deemed negligible. This threshold corresponds to an approximate susceptibility value of 0.01, representing the land least susceptible to instability. Landslide susceptibility was not modelled for LCDB-mapped urban areas due to insufficient data, thus landslide erosion was not estimated for these areas.

3.2.2 Surface erosion sub-model

In the application of the non-LiDAR version of SedNetNZ to the Waikato region (Vale & Smith, 2024), surface erosion (i.e. sheet and rill erosion from raindrop impacts and overland flow) was represented by the New Zealand Universal Soil Loss Equation (NZUSLE; Dymond et al. 2010):

$$ES = aP^2KLSC \tag{3}$$

where ES denotes surface erosion in t km⁻² yr⁻¹; a is a constant (t km⁻² yr⁻¹ mm⁻²) calibrated against measurements (Dymond et al. 2010) with a value of 1.2×10^{-3} ; P is mean annual rainfall (mm); K is the soil erodibility factor (dimensionless); L is the slope length factor; S is the slope steepness factor; and C represents the impact of vegetation cover (dimensionless) (1.0 for bare ground, 0.01 for pasture, and 0.005 for forest and scrub).

We used a revised representation of surface erosion processes, following Smith, Herzig et al. (2019), which replaced the slope length and slope steepness factors. The uniform slope length factor (L) of the NZUSLE (Dymond et al. 2010) was replaced with a factor that better represented the effect of topography on the size of convergent upslope areas contributing overland flow and surface erosion, as described by Desmet and Govers (1996):

$$L = \frac{(A + D^2)^{m+1} - A^{m+1}}{D^{m+2} \times x^m \times 22.13^m}$$
(4)

where L is the slope length factor for a given raster cell (pixel), A is the upstream catchment area (m²) at the cell inlet, D is the raster cell width (m), m is the slope length exponent, and $x = \sin a + \cos a$, with α being the slope aspect.

The slope length exponent, m, was calculated based on the rill to inter-rill ratio, β , and the slope gradient, θ (Foster et al. 1977; McCool et al. 1989, cited in Renard 1997):

$$\beta = \frac{\sin \theta / 0.896}{3 \times (\sin \theta)^{0.8} + 0.56} \tag{5}$$

$$m = \frac{\beta}{1 + \beta} \tag{6}$$

We also applied a revised slope factor, S, which is calculated according to a threshold in slope gradient SP (%) (Renard 1997):

$$S = \begin{cases} 10.8 \times \sin \theta + 0.03 & with sp < 9\% \\ 16.8 \times \sin \theta - 0.5 & with sp \ge 9\% \end{cases}$$
 (7)

Furthermore, we applied a revised, spatially variable K factor in the NZUSLE developed in Neverman et al. (2021) to better represent the spatial variability of soil erodibility, using the Fundamental Soil Layers (FSL) to represent soil parameters. We adapted the K factor equations in Wang et al. 2001 and Yang et al. 2018 to the NZUSLE:

$$K = \frac{2.1(12 - OM)M^{1.14}10^{-4} + 3.25(SS - 2) + 2.5(PP - 3)}{7.59 \times 10}$$
(8)

where OM is the soil organic matter content, M is the particle size parameter, SS is the soil structure code, and PP is the soil profile permeability code. We used six PP classes, adapted from Rosewell & Loch 2002. The soil structure code was set at SS = 2 because the FSL has insufficient data on soil structure to relate to the SS classes used for calculating K. We found the magnitude of K was not sensitive to the choice of SS class value. M was calculated as a function of the proportion of silt and clay:

$$M = Silt(100 - Clay) \tag{9}$$

where Silt and Clay are the percentage of silt and clay in the soil, respectively.

Silt was limited to a range of 15%–70%, and OM was capped at 4% to fit the nomograph of Wischmeier et al. (1971) used to derive Equation 6 for organic soils. Where there was no FSL information available to calculate a spatially varying K factor, a uniform value of 0.25 was used (Dymond et al. 2010).

Implementation of RUSLE using the LIDAR-derived DEM

In the LiDAR-based version of SedNetNZ, we replaced the NZUSLE with RUSLE (Renard et al. 1997) to better reflect the influence of rainfall erosivity on surface erosion. RUSLE and the earlier Universal Soil Loss Equation (USLE) (Wischmeier & Smith 1978) are empirical models developed using an extensive erosion data set obtained from plot measurements on predominantly agricultural land (Renard et al. 1997). The USLE/RUSLE was originally developed in the United States and has since been widely applied globally, including in New Zealand using the national 15 m DEM (Donovan 2022).

Most terms in the revised version of the NZUSLE described above are the same as those used in RUSLE, except the term representing the influence of rainfall on surface erosion rates. To fully implement RUSLE within the LiDAR-based version of SedNetNZ, we replaced aP^2 in Equation 3 with a spatial input for rainfall erosivity (Smith et al. 2024). We also excluded channel areas based on the new digital stream network from surface erosion estimates.

Rainfall erosivity (*R*) refers to the power of rainfall available to drive erosion at the soil surface (Nearing et al. 2017). The spatial distribution in annual rainfall erosivity was previously estimated across New Zealand by Klik et al. (2015) using high-temporal-resolution (10-min interval) rainfall data from 35 stations to calculate the product of total kinetic energy and maximum 30-min rainfall intensity for all rainstorms over the years of record (Klik et al. 2015). Regression analysis was used to derive climatic region-specific relationships between the estimates of rainfall erosivity and

annual precipitation (Klik et al. 2015). We used the regional relationships described in Klik et al. (2015) to estimate rainfall erosivity across the Waikato CEM catchments.

We have replaced the previous aP^2 term, which was computed using the Land Environments of New Zealand (LENZ)—based estimate of mean annual rainfall (1950–1980) (Leathwick et al. 2003), with rainfall erosivity derived using the more recent estimate of mean annual rainfall for the period 1981-2010 that was produced for the Ministry for the Environment.

Stocking density—adjusted K factor

The effect of livestock treading and grazing on surface erosion was incorporated into the LiDAR-based version of SedNetNZ through an adjustment to the surface erodibility factor (K factor in Equation 3), using the approach of Donovan and Monaghan (2021). This approach represents soil damage due to livestock activity via changes in soil permeability (ΔP_{tr}) and structure (ΔS_{tr}), which are components of the K-factor. The changes in permeability and structure were parameterised based on grazing intensity, soil moisture, clay content, and soil susceptibility to compaction and pugging according to the following equations:

$$\Delta P_{tr} = 1 + \left(p - \left(p \left(1 - 0.05 \left(hd^{0.5} \right) \right) e^{-0.5 i\omega_c} \right) \right)$$
 (10)

$$\Delta S_{tr} = 1 + \left(p - \left(p \left(1 - 0.05 \left(h d^{\{0.5\}} \right) \right) e^{-0.5 i \omega_p} \right) \right) \tag{11}$$

where ΔP_{tr} and ΔS_{tr} reflect the 'soil damage' represented via the soil permeability (PP) and structural vulnerability (SS) parameters in the RUSLE K-factor (Equation 3); p is normalised average stock hoof pressure (kPa/kPa) with values of 0.38 for sheep, and 0.7 for cattle (Fig. 2A in Donovan & Monaghan 2021); h reflects the grazing history (successive years), set to a constant 6 years, the longest reported by Donovan and Monaghan 2021 (see their Fig. 2B); d is the grazing duration, expressed as the fraction of time across the season (0-1, unitless). A value of d =1 was applied, reflecting consistent seasonal grazing practices; i is grazing intensity (relative stock unit, RSU m $^{-2}$) as derived from Equation (12), and ω_c and ω_p are soil susceptibility factors for compaction and pugging, respectively (Equations 13 & 14).

We assumed a value of d=1 based on Donovan and Monaghan (2021), reflecting consistent grazing durations at the seasonal timescale, which align with typical pasture management practices in New Zealand. This has some justification given the age of the underlying AgriBase® data is at least 3 years old, and both land use changes and the average lifespan of a farm typically occur over much longer time frames. Moreover, soil damage appears to be relatively insensitive to variations in h, particularly at higher grazing intensities (Donovan & Monaghan 2021).

Donovan and Monaghan (2021) describe grazing intensity (i) as a function of grazing density (g, head/ha) and a relative stock unit (RSU) constant (c). While Donovan and Monaghan (2021) provide typical RSU constants (c), they emphasise locally informed values are preferred to refine RSU values for specific stock types. For the four CEM catchments, WRC provided local stock unit densities (SUD) derived from AgriBase® stock numbers and these are substituted for (gc) in Equation 12.

$$i = \frac{gc}{10.000} = \frac{SUD}{10.000} \tag{12}$$

Compaction susceptibility (ω_c) and pugging susceptibility (ω_p) were modelled according to the following equations:

$$\omega_c = -0.003 \,\phi \big(75\sigma - 20(\phi + 1)\big)^2 + 8\phi + 2 \tag{13}$$

$$\omega_n = 1 - e^{-500\phi(max(0, \sigma^3 - 0.25\phi))^2}$$
(14)

where, (ϕ) is the clay content (0-1) from the FSL clay value in Equation 9; and σ is the soil water content (SWC). In the absence of high-resolution spatial data, Donovan and Monaghan (2021; their Fig. 2D) estimated seasonal averages for SWC using data from New Zealand soil measurements (Curran-Cournane et al. 2011; Laurenson et al. 2016). We used the mean of these seasonal averages to derive an annual estimate ($\sigma = 0.325$).

3.2.3 Riverbank erosion sub-model

The total mass of material eroded from riverbanks each year was modelled as a function of bank height, reach length, and bank migration rate (Dymond et al. 2016):

$$B_i = \rho M_i H_i L_i \tag{15}$$

where B_j is the total eroded mass for the j^{th} stream segment (t yr⁻¹), ρ is the bulk density of the bank material (t m⁻³), M_j is the bank migration rate (m yr⁻¹), H_j is the mean bank height (m) and L_j is the length (m) of the j^{th} stream segment.

The predicted mass of material eroded from riverbanks represents the gross contribution of sediment supplied to the river channel per year. This does not account for redeposition and storage of eroded bank material on banks, within the channel bed or the lateral accretion of material on bars with channel migration. Hence, net bank erosion in SedNetNZ was previously estimated as one-fifth of gross bank erosion, based on reach-scale sediment budgets comparing bank erosion and accretion (De Rose & Basher 2011).

In earlier applications of SedNetNZ, bank migration rate was predicted using a simple empirical relationship between mean annual flood and bank migration rate (Dymond et al. 2016). This earlier version was replaced by an improved sub-model to better represent the spatial variability in factors influencing bank migration (Smith, Spiekermann et al. 2019). Factors in this sub-model included mean annual flood (MAF), channel slope, channel sinuosity, soil texture-based erodibility, valley confinement, riparian woody vegetation, and bank protection works (Smith Spiekermann et al. 2019). The application of this improved sub-model in the Waikato region was described by Vale & Smith (2024).

Subsequently, a new data-driven riverbank erosion sub-model was developed by Smith et al. (2024). This sub-model focused on improving estimates of: a) bank migration rates; b) bank heights that are required to convert bank migration rate to gross bank erosion; and c) storage of eroded bank material within channels to estimate the net contribution of bank erosion to sediment loads. The new sub-model was based on an expanded data set of reach-averaged lateral bank migration rates (m yr⁻¹) obtained by mapping channel planform change from repeated aerial imagery across the Hawke's Bay and Greater Wellington regions. This mapping increased the length of channel with data available for model training from 77 to over 800 km (Smith et al. 2024).

Bank migration rates

Previously Smith et al. (2024) compared the predictive performance of four sub-models to estimate bank migration rates using inputs derived from LiDAR DEMs. Of the four tested, the random forest (RF) model produced the least error (i.e. root mean square error [RMSE] and mean absolute error [MAE], both expressed in units of m yr^{-1}) in model fitting (RMSE = 0.15, MAE = 0.06) and prediction (RMSE = 0.31, MAE = 0.14) using the expanded bank migration data set. The RF also outperformed the bank erosion sub-model previously applied in the Waikato region (Smith et al. 2024). Therefore, the fitted RF model was applied to predict reach-averaged bank migration rates for stream segments in the digital networks of the four CEM catchments.

For use in the RF sub-model, MAF was estimated across the LiDAR DEM-derived digital stream network in each catchment using a fitted power function ($MAF = 26q^{0.61}$; R² = 0.97; n = 35) between modelled mean annual discharge (q) and MAF measured at river gauging stations in the Waikato region (Vale & Smith 2024). Mean annual discharge for each link in the REC2 digital network was previously estimated by Woods et al. (2006) and Elliott et al. (2016) using an empirical water balance model. These estimates of discharge ($m^3 s^{-1}$) were converted to runoff ($mm yr^{-1}$) and used to re-compute mean annual discharge for the LiDAR DEM-derived digital network based on the upstream contributing area of each stream segment. Channel slope, channel sinuosity and valley confinement were computed using the 5 ha digital stream network and the 5 m LiDAR DEM. Soil textured-based erodibility was estimated from soil textural classes compiled from the Fundamental Soil Layers (Newsome et al. 2008; Vale & Smith 2024).

The proportion of riparian woody vegetation per digital stream segment was estimated using a canopy height model (CHM) obtained by differencing the LiDAR-derived 1 m digital surface model (DSM) and DEM with a minimum height of 2 m to represent established woody vegetation. The higher resolution CHM replaced a classified map of 2002 woody vegetation cover derived from Landsat TM at 15 m resolution (Dymond & Shepherd 2004) that was previously used in the region-wide modelling (Vale & Smith 2024).

Bank height

Estimates of reach-average bank height are needed to predict the suspended sediment contribution from riverbank erosion (Equation 15). In earlier applications of SedNetNZ, mean bank height (H_j) for each stream segment was estimated from a simple regional relationship with mean annual discharge (Dymond et al. 2016). This produced a bank height that increased downstream with discharge, and did not account for reach-to-reach variations in bank height that reflected local river channel form. In the upgraded sub-model, we estimate bank heights directly from a LiDAR-derived 1 m DEM. The new approach estimated bank heights from transects located perpendicularly to the digital stream network at 50 m intervals. The width of transects varied per stream segment as a function of mean discharge and the inverse of mean lateral slope (as a proxy for valley confinement) to approximate variations in bankfull width (Smith et al. 2024).

This approach for estimating bank heights showed significant improvement compared to the previous approach based on mean annual discharge when assessed using manual point-based height measurements averaged at the reach scale. For example, the coefficient of determination (R^2) relative to the 1:1 line increased from 0.40 to 0.66 for estimates of mean bank height based on

mean annual discharge versus the LiDAR based approach, respectively, for streams in the Hawke's Bay region (Smith et al. 2024).

Net bank erosion

Estimating the net contribution of bank erosion to suspended sediment loads requires information on the redeposition and storage of eroded bank material on banks, within the channel bed; or on the lateral accretion of material on bars with channel migration. Such information is not widely available. In early applications of SedNetNZ, net bank erosion was estimated at one-fifth of gross bank erosion – based on results from a detailed empirical study using repeated aerial photography and LiDAR surveys in the Waipaoa River catchment (De Rose & Basher 2011).

Subsequently, net bank erosion was estimated from extensive channel planform mapping in the Hawke's Bay region for comparison with the previous Waipaoa-based estimate (Smith et al. 2024). Planform mapping identified areas of both erosion and accretion within channels for each digital stream segment which were converted to mean annual rates of reach-average lateral erosion or accretion (m yr⁻¹). Average erosion and accretion volumes per segment per year were then approximated using the average of the maximum and minimum mapped bank heights per transect, respectively. This planform mapping analysis assumed that, for laterally migrating channels, the outer eroding bank is typically higher than the opposite accreting bank. In practice, bank heights may vary between erosion and accretion zones, while some reaches may experience erosion or accretion along both banks. Nonetheless, this assumption provided a first-order approximation for estimating net bank erosion based on a significantly larger data set (805 km of channel length) for comparison with the previous estimate based on 44 km of mapped channel length in the Waipaoa catchment.

Net bank erosion as a proportion of gross bank erosion was estimated at 0.28 based on the channel planform and bank height mapping data from Hawke's Bay (Smith et al. 2024). This is comparable to the 0.20 estimate used in previous SedNetNZ modelling. While both estimates are subject to considerable uncertainty, their consistency suggests that these values may provide a reasonable approximation for determining net bank erosion in the absence of repeated LiDAR surveys.

Suspended sediment loads from bank erosion

The RF sub-model was fitted 100 times (mean $R^2 = 0.87$) using all available bank migration data and the resulting mean predicted bank migration rate per stream segment was used in each CEM catchment. We then combined these mean predictions of bank migration rates with the LiDAR-based estimates of mean bank height per stream segment, and the revised estimate of net bank erosion to estimate mean annual net suspended sediment load from bank erosion per stream segment in each catchment.

3.2.4 Sediment routing and floodplain storage

SedNetNZ estimates the mean annual suspended sediment load delivered by each erosion process to the digital stream network. This sediment is then routed through the network to the coast. Previously, sediment deposited on floodplains was assumed to spread evenly across the floodplain for each major river catchment (Dymond et al. 2016). However, in the latest application of SedNetNZ to the Waikato region (Vale & Smith 2024), a revised floodplain deposition algorithm was applied to estimate the amount of sediment entering floodplain storage along the stream network based on upstream loads rather than averaging the load deposited on floodplains across major catchments (Vale et al. 2021).

In the revised algorithm, the mass of sediment (t yr⁻¹) entering floodplain storage in the ith subwatershed (F_i) is calculated as:

$$F_i = pS_t \frac{L_i acc S_i^2}{\sum L_i acc S_i^2} \tag{16}$$

where p is the proportion of the sediment load generated by hillslope erosion per lake or seadraining catchment that is deposited on floodplains in the catchment, set to 5% based on previous SedNetNZ parameterisation carried out in the Manawatū (Dymond et al. 2016), S_t is the total sediment load (t yr⁻¹) generated by hillslope erosion per lake or sea-draining catchment, L_i is the segment length (m) on floodplain in the ith subwatershed, and $accS_i$ is the total accumulated (upstream) sediment load from hillslope erosion (t yr⁻¹) in the ith subwatershed.

Previous applications of the non-LiDAR based version of SedNetNZ used the NZLRI to define the spatial extent of floodplains. The NZLRI was mapped at a scale of 1:63,360 and may not capture smaller areas of floodplain. In the present work, we use the LiDAR-derived 5 m DEMs for the Waikato CEM catchments to identify the extent of floodplains along the digital stream network. We did not seek to model the area of floodplain inundated by the largest flood on record. Instead, we represented the length of channel where flows may go overbank and deposit sediment on floodplains on average over a multi-decadal period (i.e. L_i in Equation 16). Therefore, we defined floodplains as areas of low slope land adjacent to the active channel which may be inundated by the average annual maximum flow.

Smith et al. (2024) estimated the depth of the average annual maximum flow across stream orders (1–8) using the annual maximum flow from 77 water level gauges in Hawke's Bay, with a mean record length of 27 years. Based on this analysis, the estimated maximum floodplain height above the channel ranged from 1–5 m depending on the stream order. These values were used to identify subwatersheds where sediment may enter floodplain storage. We applied the same criteria to determine the floodplain extent in the Waikato CEM catchments, using height above nearest drainage (HAND) to identify floodplain. The stream bed and banks were excluded from the floodplain extent using a 7.5 m buffer either side of the streamlines (i.e. for a total width of 3 pixels), and a slope threshold of 5 degrees.

To account for sediment trapping through lakes, we applied a lake-specific sediment passing factor (*SPF*) to the net sediment load at the end of a subwatershed draining to a lake. We calculated *SPF* using an adaptation of Gill's (1979) approximation of Brune's (1953) trap efficiency (the inverse of passing factor) curve for medium sediment:

$$SPF = 1 - \frac{V/I}{1.02(V/I) + 0.012} \tag{17}$$

where V is the lake volume, and I is the annual inflow to the lake.

3.3 Model simulations

3.3.1 Scenario overview

Contemporary baseline

The contemporary baseline scenario (C2023) represents recent land cover (LCDB v5, 2018) and erosion mitigations (soil conservation works) completed to date based on data provided by WRC. We use data from the CEM catchment riparian surveys (survey dates range from 2020 to 2024) to estimate the proportional extent of riparian fencing for each segment in the digital stream network derived from the LiDAR-based 5 m DEM, and include existing riparian retirement from spatial data provided by WRC. Existing soil conservation works on hillslopes (including indigenous retirement, protection production plantings, and space-planted trees) are represented using the spatial data supplied by WRC. We also include the stock density data supplied by WRC derived from AgriBase® in the surface erosion sub-model to represent the effect of livestock treading on soil erodibility.

Future erosion mitigation scenarios

The mitigation scenarios quantify the effect of future erosion mitigations on suspended sediment loads in each of the four CEM catchments. The scenarios represent erosion mitigations as fully implemented and fully matured. After discussion with WRC we agreed to implement two scenarios.

Mitigation scenario 1 (M1):

- Retirement and afforestation: pastoral land on slopes ≥ 35° are retired and transitioned to permanent woody vegetation cover (native or exotic), based on the LiDAR-derived 5 m DEM.
- Space-planted trees: pastoral land on slopes ≥ 26° and < 35° remains in production with implementation of space-planted trees.
- Riparian stock-exclusion fencing: stock-exclusion fencing and setback distances are defined according to the rules described in Regional Plan Change 1 (Waikato Regional Council [WRC] 2020).

Mitigation scenario 2 (M2):

- Retirement and afforestation: pastoral land on slopes ≥ 30° are retired and transitioned to permanent woody vegetation cover (native or exotic), based on the LiDAR-derived 5 m DEM.
- Space-planted trees: pastoral land on slopes ≥ 26° and < 30° remains in production with implementation of space-planted trees.
- Riparian stock-exclusion fencing: stock-exclusion fencing and setback distances are defined according to the rules described in Regional Plan Change 1 (WRC 2020).

For Mitigation scenarios 1 and 2, we ranked subwatersheds from highest to lowest based on the proportion of pastoral land with slopes \geq 35° or \geq 30° (depending on the scenario) in each catchment and sequentially targeted 20%, 30%, 40%, 50% and 100% of these areas for conversion to permanent woody cover. In parallel, we applied the same approach for slopes \geq 26° to < 35° or < 30° (depending on the scenario), and sequentially target 20%, 30%, 40%, 50% and 100% of these areas for conversion to space-planted trees.

We also ran model simulations to assess the effect of the full implementation of each erosion mitigation type when applied individually for both Mitigation scenarios 1 and 2. These scenarios and their names are summarised in Table 3. A summary of the estimated area of works and length of fencing is provided in Table 4.

Table 3. Summary of mitigation scenarios and their names

	Scenario description (% implementation)		Mitigation scenario 1 (M1)	Mitigation scenario 2 (M2)
Combined	% of pastoral area with slope threshold	20%	M1_20	M2_20
mitigation scenarios	(≥ 35° /≥ 30° for permanent woody cover; ≥ 26° to ≥ 35° /≥ 30° for space-planted trees)	30%	M1_30	M2_30
scenarios		40%	M1_40	M2_40
		50%	M1_50	M2_50
		100%	M1_100	M2_100
Individual	Retirement and afforestation	100%	M1_aff	M2_aff
mitigation types*	Space-planted trees	100%	M1_spa	M2_spa
	Riparian stock-exclusion fencing	100%	M1_rip	M2_rip

^{*}Individual mitigation types are fully implemented

Table 4. Summary of the area or length of erosion mitigation works applied under each scenario

CEM catchment	Scenario	Retirement and Afforestation (ha)	Space-planted Trees (ha)	Riparian stock-exclusion fencing (km, % of network)
Kaniwhaniwha	M1	137	444	20 (00/)
Kaniwhaniwha	M2	321	260	38 (9%)
Varanira	M1	76	362	FC (100/)
Karapiro	M2	200	238	56 (18%)
Matahawa	M1	470	1,118	1.42 (2.40/)
Matahuru	M2	1,005	583	142 (34%)
Moakurarua	M1	676	1,641	112 /150/)
ivioakurarua	M2	1,451	866	112 (15%)

3.3.2 Estimating sediment load reductions from mitigation works

Reduction in hillslope erosion from mitigation works

The reduction in sediment load from hillslope erosion processes is determined by the change in land cover related to the mitigation work in each scenario. The total reduction is determined by the effectiveness and maturity of each type of erosion mitigation. Effectiveness represents the capacity of the erosion mitigation to reduce sediment load once fully mature and is specific to each mitigation, while the maturity represents the proportion of time passed relative to the age at which a mitigation may be considered fully mature and thus fully effective. Maturity rates are outlined in Table 5 and based on values used in previous work (e.g. Douglas et al. 2008; Manderson et al. 2011; McIvor et al. 2011; Basher et al. 2018). The effectiveness and maturity values used in our modelling are simplified representations based on published data and assume that mitigation works are fully implemented and fully effective. These assumptions may tend to represent best-case outcomes, as the literature reports a wide range of effectiveness values for different erosion control works, and real-world performance can vary considerably.

Past, present, and future erosion mitigation works, and the related changes to land cover, are represented in the model. Spatial data on the past and present erosion mitigation works were supplied by WRC in the form of soil conservation data for the four CEM catchments. This provided information on the spatial extent, type, and year of implementation of soil conservation works. The types of soil conservation work were matched to the erosion mitigation types represented in the model (Table 5), and the year of implementation and rate of maturity were used to determine the maturity of the works for the contemporary baseline. In the future mitigation scenarios, works are represented as fully matured.

Conversion to permanent woody cover has an effectiveness value of 90% for mass movement erosion based on published data (Phillips et al 2020; Dymond et al. 2006; Page et al. 1999; Pain & Stephens 1990; Bergin et al. 1993, 1995; Phillips et al. 1990; Marden & Rowan 1993; Marden et al 1991). Space-planted trees and gully tree planting have a value of 70% based on data from Hawley and Dymond (1988), and consistent with Douglas et al. (2009, 2013; McIvor et al. (2015), although the various studies report varying effectiveness (see model limitations). The effectiveness of afforestation and bush retirement in reducing surface erosion (Table 5) was derived from the change in C in equation 3 based on the conversion of pasture to forest/scrub. Space-planted trees and gully tree planting do not typically achieve canopy closure, and therefore reductions from these mitigations were not applied to surface erosion. Riparian retirement was applied to mitigate bank erosion with a reduction of 80% attributable to riparian fencing and stock-exclusion (Dymond et al. 2016; Phillips et al 2020), although we recognize that published studies report a range of effectiveness values (see discussion in section 4.4 on model limitations).

Table 5. Summary of maturity and effectiveness of the erosion mitigation works on pasture used in the modelling

Erosion mitigation	Years to fully mature	Annual maturity rate	Effectiveness	Soil conservation asset type from WRC data
Conversion to woody cover (afforestation/ bush retirement)	10	10%	90% (mass movement) 50% (surficial)	'Indigenous Retirement', 'Protection Production Plantings'
Space-planted trees	15	6.66%	70% (mass movement)	'Space Planting'
Riparian retirement	2	50%	80% (bank erosion)	'Riparian Retirement', 'Stream Bank Erosion Control Plantings'

^{*}Maturity and effectiveness rate are derived and summarised from Basher et al. 2018, Douglas et al. 2008; McIvor et al. 2011

Reduction in hillslope sediment delivery to streams from surface erosion

A sediment passing factor, the inverse of trapping efficiency, was calculated for the riparian buffer of the *j*th stream segment (PF_{F_i}) following Zhang et al. (2010):

$$PF_{F_j} = 1 - \frac{k(1 - e^{-bw})}{100} \tag{18}$$

where k and b are fitted parameters equal to 90.9 and 0.446, respectively (Zhang et al. 2010), and w is the buffer width. We estimated a mean buffer width for each digital stream segment based on the proportion of land class and the corresponding buffer width intersecting with the segment. The proportion of fencing in each stream segment, and the mean buffer width was determined using data from the WRC CEM riparian survey (described in next paragraph) Riparian fencing was applied to the future scenarios based on Schedule C of the Proposed Waikato Regional Plan Change 1 (WRC, 2020).

The reduction in sediment load delivered from surface erosion due to fencing and stock-exclusion from riparian retirement in a reach (S_{F_j}) is a function of the proportion of the reach fenced (FR_j) and the buffer passing factor:

$$S_{F_i} = ES_j \times \left(1 - FR_j PF_{F_i}\right) \tag{19}$$

where ES_i is the load from surface erosion for the j^{th} reach per subwatershed.

Reduction in bank erosion

The reduced sediment load from bank erosion due to fencing and stock-exclusion (B_{F_j}) was calculated as:

$$B_{F_j} = B_j \times \left(1 - 0.8FR_j\right) \tag{20}$$

where B_j is the net suspended sediment load from bank erosion without the effect of fences reducing erosion. A sediment load reduction of 80% from bank erosion may be attributable to

riparian fencing and stock-exclusion (Dymond et al. 2016; Phillips et al. 2020). This reflects the effect of reduced stock trampling and foraging on banks (Trimble 1994), as well as the potential for riparian woody vegetation to become better established in the absence of livestock over the longer term. The estimated 80% reduction assumes the buffer strip is no longer grazed and sufficient time has elapsed for banks to recover from previous trampling impacts, and for woody vegetation to become established and increase bank stability (see discussion in Section 4.4.2).

Riparian fencing estimates

The proportion of riparian fencing was estimated using CEM catchment riparian survey data provided by the WRC. Previously, region-wide riparian survey data from 2002, 2007, 2012, and 2017 – established to monitor changes in fencing and vegetation on selected pastoral sites across the Waikato region (Norris et al. 2020), was used in the region-wide SedNetNZ modelling (Vale & Smith 2024).

For the present application, CEM catchment-specific riparian surveys conducted between 2020 and 2024 were provided by WRC for the four CEM catchments (Norris & Norris 2021; Norris 2022; Norris et al. 2023). The CEM surveys are largely the same as the regional riparian characteristics surveys, employing a stratified random sampling design to represent variations in land use and stream order. Each survey site spanned a 500 m stretch of waterway, with visual assessments conducted on both banks to evaluate various parameters, including fencing and buffer width (Norris & Norris 2021).

A similar approach to that used by Vale & Smith (2024) was applied in the present study to estimate the proportion of riparian fencing and buffer widths per stream segment, with adjustments reflecting differences in sample size and spatial characteristics from the CEM survey data. Survey data from the four CEM catchments were combined, and site data processed to derive fencing proportions and mean buffer widths for each site. These proportions and widths were then summarised by stream order (1 to \geq 6) and land use/farm type (i.e. drystock or dairy) to enable spatial application across the digital stream network (Table 6).

The criteria reflect the main variables informing the survey design (e.g. land use and stream order) and account for factors influencing spatial variation in riparian fencing, while maintaining adequate sample sizes for each stream order and farm type combination ($n \ge 6$, except for one group; most sample sizes ranged between 10 and 30). Additionally, a CEM-specific weighting (based on the average fencing proportion or buffer width for each CEM) was applied to account for differences in fencing extent across the CEM catchments, beyond land use and stream order.

Table 6. Summary of estimated fencing proportions at different catchments for the digital stream network based on CEM riparian surveys

Stream	nm Farm type Estimated fencing proportions		Mean buffer width (m)						
order		Kaniwhaniwha	Karapiro	Matahuru	ı Moakurarua	Kaniwhaniwha	Karapiro	Matahuru	Moakurarua
1	Dairy	89%	71%	66%	88%	2.5	3.6	1.8	2.9
	Drystock	33%	38%	18%	26%	3.8	4.8	1.5	2.6
2	Dairy	87%	69%	64%	85%	2.6	3.7	1.9	3.1
	Drystock	36%	42%	20%	28%	2.8	3.6	1.1	2.0
3	Dairy	97%	90%	84%	97%	1.6	2.3	1.2	1.9
	Drystock	35%	40%	19%	27%	2.8	3.5	1.1	1.9
4	Dairy	93%	86%	80%	93%	3.7	5.3	2.7	4.4
	Drystock	51%	59%	28%	40%	4.0	5.0	1.5	2.8
5	Dairy	90%	72%	67%	89%	4.6	6.7	3.4	5.5
	Drystock	89%	100%	48%	70%	6.3	7.9	2.4	4.4
≥6	Dairy	100%	80%	75%	99%	5.3	7.6	3.8	6.3
	Drystock	96%	96%	58%	84%	7.9	10.0	3.0	5.5

Land use associated with the digital stream network segments was determined using AgriBase® spatial data provided by the WRC, in combination with LCDB v5, to exclude areas unsuitable for riparian fencing (e.g. indigenous forest areas). Riparian fencing estimates were not applied to small headwater tributaries (stream order = 1) outside the 15° low-slope area (described below) and classified as 'narrow' streams under the Sustainable Dairying Water Accord's definition of 'Accord streams' (Dairy Environment Leadership Group 2013). The 'Accord streams', determined for the REC2 network, were mapped onto the LiDAR-based digital stream network. These streams are defined as being wider than 1 m, deeper than 30 cm, and having permanent flow. Stream widths were estimated using mean annual flow data for each REC2 segment (Booker & Hicks 2013; Semadeni-Davies & Elliott 2016; Whitehead & Booker 2020).

Riparian fencing was applied to the future scenarios based on Schedule C of the Proposed Waikato Regional Plan Change 1 (WRC 2020). This specifies that farmed cattle, horses, deer, and pigs are to be excluded from water bodies on land with a slope of up to 15°; or, with a slope over 15° where any paddock adjoining the water body have stock unit numbers exceeding 18 per grazed hectare at any time. Future fencing was not applied to stream segments with a stream order = 1 and classified as 'narrow' streams under the Sustainable Dairying Water Accord's definition of 'Accord streams'.

Slope was derived from the LiDAR-based 5 m DEM and stock unit numbers based on AgriBase® provided by WRC. The slope layer was processed to improve the continuity of low-slope areas and ensure suitable alignment with the digital stream network and stock unit density layer. Processing included applying a majority filter, boundary cleaning, and removing small areas below a minimum area threshold of 400 m^2 ($20 \text{ m} \times 20 \text{ m}$). Subsequently, a 10 m buffer was applied around the digital stream network to capture stream segments with adjacent low-slope paddock areas.

New riparian fencing was implemented with a setback distance of 3 m from water bodies and 1 m from drains, except for drains <2 m, reflecting Regional Plan Change 1 requirements. However, other catchment initiatives may specify different setbacks (e.g. 5 m setbacks under incentivised management programmes) which were not considered here. Due to the absence of high-resolution spatial data or explicit drain designations in the digital stream network, we applied a 3 m setback distance to all new riparian fencing, except for stream segments with a stream order \ge 2 classified as 'narrow' streams under the Sustainable Dairying Water Accord's definition of 'Accord streams', where a 1 m setback is applied. Stream segments with a stream order of 1 did not have fencing applied.

3.4 Reductions for NPS-FM visual clarity attribute bands

To assess the improvement in attribute state under future scenarios, we used the approach developed by Hicks et al. (2019) to estimate the proportional change in mean annual suspended sediment load required to achieve an improved attribute state. This approach is recommended by the Ministry for the Environment in their guidance for implementing the NPS-FM 2020 sediment requirements (Ministry for the Environment 2022), and directly informed development of the suspended fine sediment attribute for the NPS-FM 2020 (see Hicks & Shankar 2020).

Following Hicks et al. (2019) and Ministry for the Environment (2022), the proportional change in mean annual suspended sediment load required to achieve a target attribute state was calculated as a function of the ratio between the current state visual clarity (visual clarity for each scenario) and the target visual clarity, using Equation 21 at the SOE site:

$$PR_{v} = 1 - (V_{o}/V_{b})^{1/a} (21)$$

where PR_v is the minimum proportional change in mean annual suspended sediment load required to achieve the target visual clarity, V_o is the target visual clarity for each attribute band (Table 7), and V_b is the current state median visual clarity. We follow the recommendation of the Ministry for the Environment (2022) and assume a in Equation 21 takes the national average reported by Hicks et al. (2019) of -0.76.

The baseline attribute state was determined using the median visual clarity calculated from the most recent 60 visual clarity observations for each SOE site in the CEM catchments, provided by WRC (Table 8). Median visual clarity requires monthly observations over a minimum record length of 5 years (60 samples). Only the SOE site in the Moakurarua does not reach this threshold (n = 51), but as it was very close, the analysis was still undertaken.

To assess the minimum proportional change in suspended sediment load required to improve the attribute band, we used the lower-bound visual clarity for each band (Table 7) for V_o ; the upper-bound was used to assess the minimum change in load required for a decline in state from a higher band.

Table 7. Attribute bands and numerical attribute states for suspended fine sediment

Attribute band and description	Numerical attribute state by suspended sediment class (visual clarity [m])					
	1	2	3	4		
A Minimal impact of suspended sediment on instream biota. Ecological communities are similar to those observed in natural reference conditions.	≥1.78	≥0.93	≥2.95	≥1.38		
B Low to moderate impact of suspended sediment on instream biota. Abundance of sensitive fish species may be reduced.	<1.78 and ≥1.55	<0.93 and ≥0.76	<2.95 and ≥2.57	<1.38 and ≥1.17		
C Moderate to high impact of suspended sediment on instream biota. Sensitive fish species may be lost.	<1.55 and >1.34	<0.76 and >0.61	<2.57 and >2.22	<1.17 and >0.98		
National bottom line (NBL)	1.34	0.61	2.22	0.98		
High impact of suspended sediment on instream biota. Ecological communities are significantly altered, and sensitive fish and macroinvertebrate species are lost or at high risk of being lost.	<1.34	<0.61	<2.22	<0.98		

Source: Reproduced from Table 8 in the NPS-FM 2020 (Ministry for the Environment 2020).

The attribute band thresholds for suspended fine sediment are determined by the 'sediment class' associated with each REC2 segment (Table 8). The sediment class of a given segment is determined by the climate, topography, and geological classification (as defined in the REC2) of upstream segments predominantly contributing flow to a given segment. We used the layer denoting suspended sediment class for the REC2 digital stream network produced by Hicks and Shankar (2020)⁴ to identify the sediment class of the segment associated with each SOE monitoring site. This was then mapped onto the stream segments from the LiDAR-based digital stream network (Figure 4).

⁴ Available from the Ministry for the Environment data portal at https://data.mfe.govt.nz/layer/103687-hydrological-modelling-to-support-proposed-sediment-attribute-impact-testing-2020/

Table 8. Summary details for SOE monitoring sites with measured median visual clarity (CLAR, m) derived from black disc measurements

CEM catchment	Site name	Site ID	REC2 nzsegment ID	Date range used	n	Sediment class	Median CLAR	Base state
Kaniwhaniwha	Kaniwhaniwha Stm at Wright Rd	222_16	3068190	Aug-2016 – Aug-2023	60	1	0.74	D
Karapiro	Karapiro Stm at Hickey Rd Bridge – Cambridge	230_5	3070130	Sep-2018 – Jun-2024	60	1	0.79	D
Matahuru	Matahuru Stm at Waiterimu Road Below Confluence	516_5	3053073	Dec-2010 – May-2016	60	2	0.29	D
Moakurarua	Moakurarua Stm at Warratah Farm Bridge	553_12	3081452	Sep-2018 – Jun-2024	51	1	0.94	D

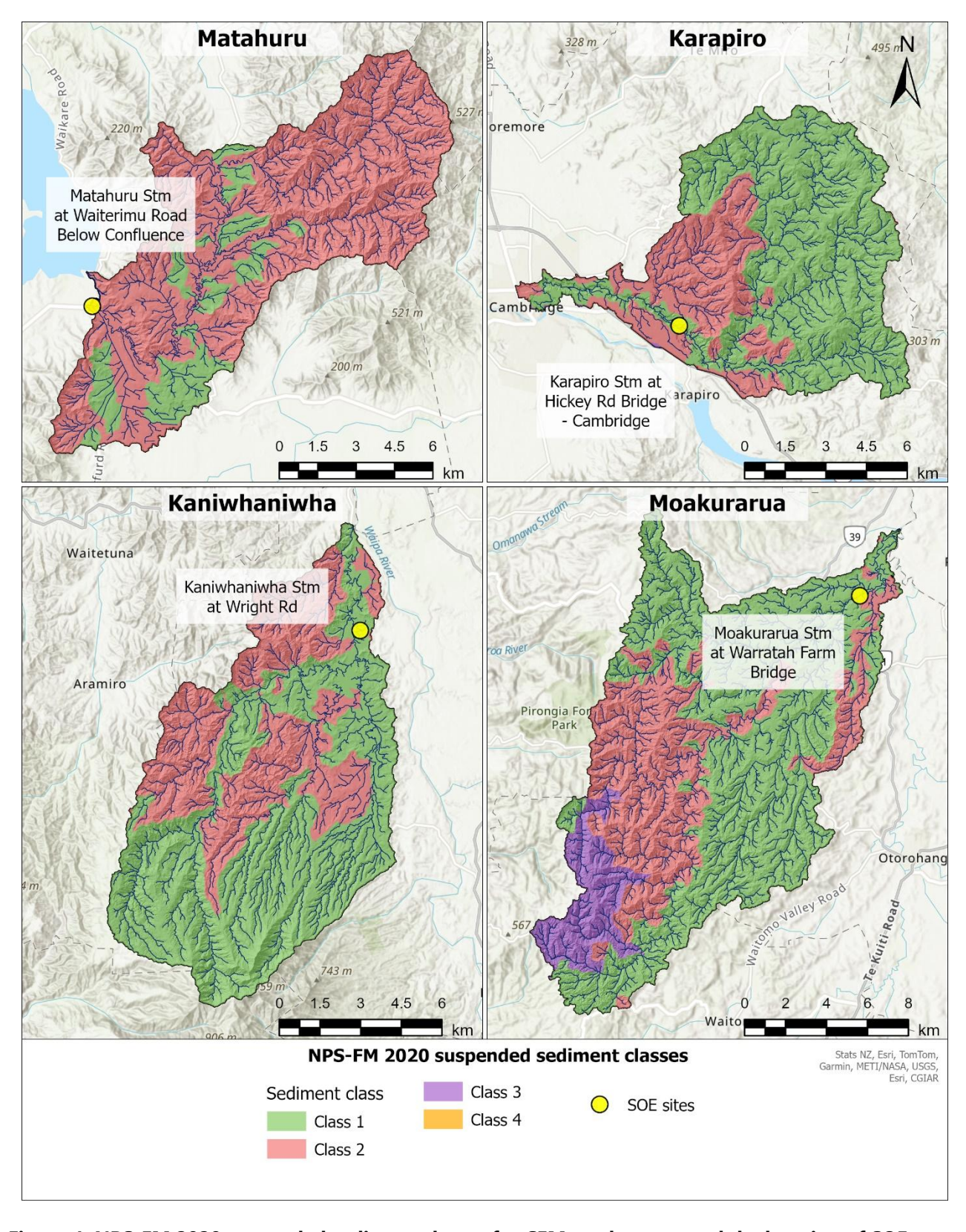


Figure 4. NPS-FM 2020 suspended sediment classes for CEM catchments, and the location of SOE monitoring sites.

4 Results

4.1 LiDAR-based SedNetNZ erosion and sediment load model for the CEM catchments

This section provides an overview of the outputs from the upgraded shallow landslide, surface and riverbank erosion sub-models under contemporary baseline conditions, then considers the catchment suspended sediment budgets for both the contemporary baseline and future mitigation scenarios. The CEM catchment layers associated with the LiDAR-based version of SedNetNZ that accompany the present report are summarised in Appendix 1.

4.1.1 Shallow landslide erosion

Shallow landslide erosion may be expressed as the mean annual sediment yield from shallow landslides delivered to the stream network. This representation of shallow landslide erosion does not imply landslide erosion occurs every year but instead averages on an annual basis the sediment load generated by discrete landslide-triggering events that occur over multi-decadal intervals. This approach allows for the construction of sediment budgets where the contributions from each erosion process may be expressed in the same units: either as suspended sediment loads (t yr⁻¹) or net sediment yields (t km⁻² yr⁻¹).

The spatial patterns in mean annual net sediment yields (per pixel) from shallow landslides are shown in Figure 5 for the four CEM catchments. These pixel-based yields form the basis for computing the shallow landslide sediment load contribution for each subwatershed in the digital stream network. The highest net sediment yields (> 1,000 t km⁻² yr⁻¹) from shallow landslide erosion occur most extensively on soft rock pastoral hill country, particularly in the eastern Matahuru catchment, and less extensively in the central areas of the Kaniwhaniwha and a limited area in the eastern Moakurarua. In contrast, the forested hard rock terrain has significantly lower net sediment yields (< 25 t km⁻² yr⁻¹) from landslide erosion, which reflects the lower susceptibility of this terrain to the occurrence of landslides (Figure 5).

The mean annual net sediment load delivered to the stream network from shallow landslide erosion amounted to 14.6 kt yr⁻¹, 12.2 kt yr⁻¹, 7.8 kt yr⁻¹, and 3.7 kt yr⁻¹ for Moakurarua, Matahuru, Kaniwhaniwha, and Karapiro, respectively, using the upgraded shallow landslide sub-model with the LiDAR-derived DEM.

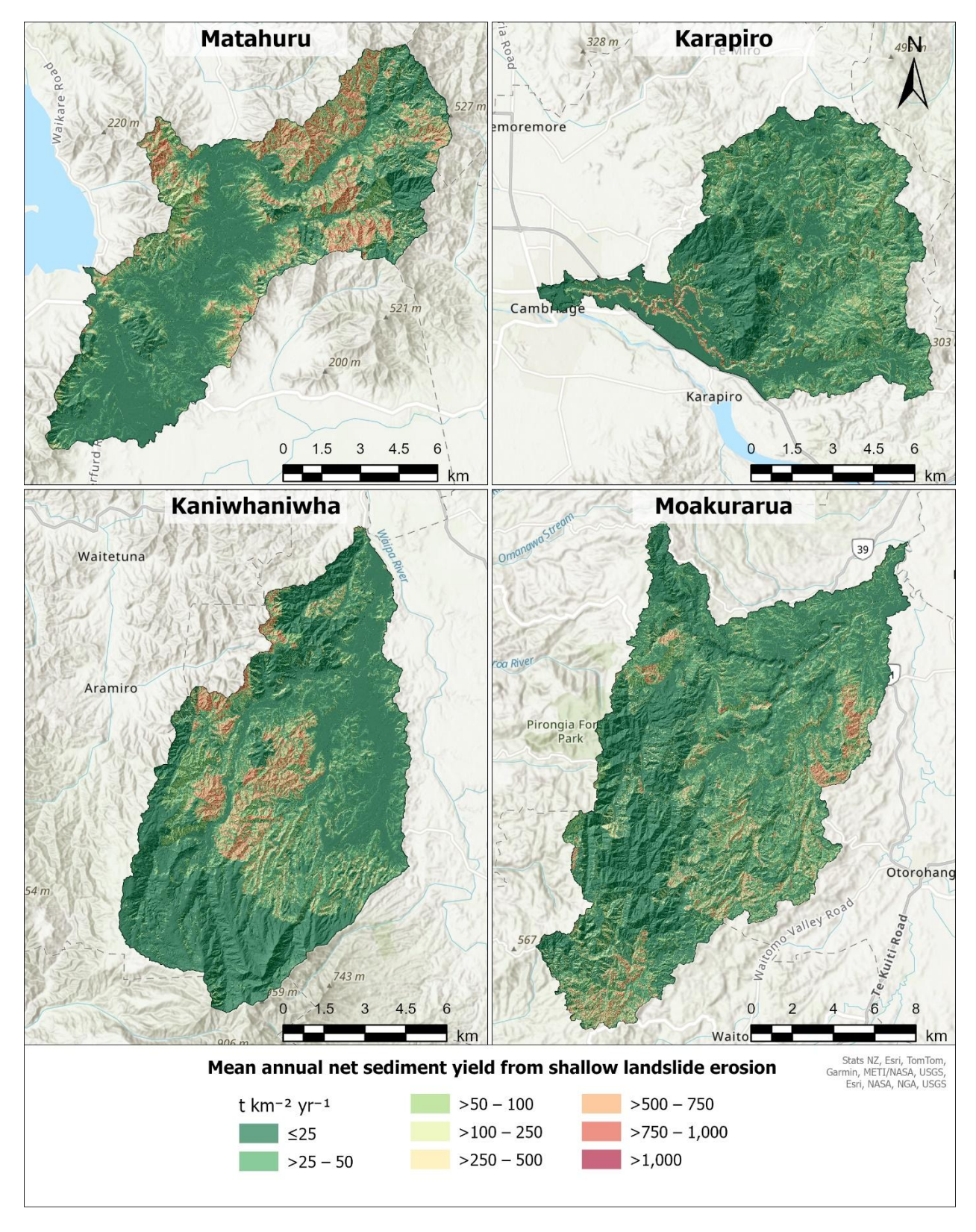


Figure 5. Mean annual net sediment yield (t km⁻² yr⁻¹) from shallow landslide erosion delivered to the stream network based on 2018 land cover from LCDB v5.0 and existing soil conservation works, displayed over the underlying hillshade layer.

4.1.2 Surface erosion

Mean annual net sediment yields from surface erosion (sheet and rill erosion) delivered to the stream network are shown in Figure 6. The spatial pattern in surface erosion reflects spatial variations in the RUSLE factors. Higher rainfall erosivity tends to occur over elevated terrain due to orographic effects that produce higher rainfall. Soil erodibility increases where surface soils have lower organic matter and higher silt content. Steep and convergent terrain concentrates surface runoff that may increase erosion, while vegetation cover has a critical role in protecting the soil surface from raindrop impact and increasing surface roughness that reduces overland flow velocities.

Within the four CEM catchments, the highest surface erosion rates (>1,000 t km⁻² yr⁻¹) tend to occur in hilly and mountainous areas with higher rainfall and steep, convergent terrain (Figure 6). Within these areas, those locations lacking vegetation cover or where soils tend to have higher silt content exhibit higher surface erosion rates. Notably, the western Moakurarua hill country exhibits particularly high surface erosion. The mean annual net sediment load delivered to the stream network from surface erosion amounted to 16.2 kt yr⁻¹, 3.4 kt yr⁻¹, 2.7 kt yr⁻¹, and 2.1 kt yr⁻¹ for Moakurarua, Kaniwhaniwha, Karapiro, and Matahuru, respectively, using the RUSLE sub-model with the LiDAR-derived DEM.

A new stocking density-adjusted *K* factor was introduced into the surface erosion sub-model to account for the effects of livestock treading and grazing on surface erosion. Incorporating this adjustment increased sediment load contributions from surface erosion by 2%–3% in Moakurarua, Karapiro, and Kaniwhaniwha, and by 10% in Matahuru, though the overall impact on catchment-wide erosion loads from all processes combined was small (0.8%–1.2%). The effect was most pronounced in areas with high stock densities, particularly on lower-slope pastoral land.

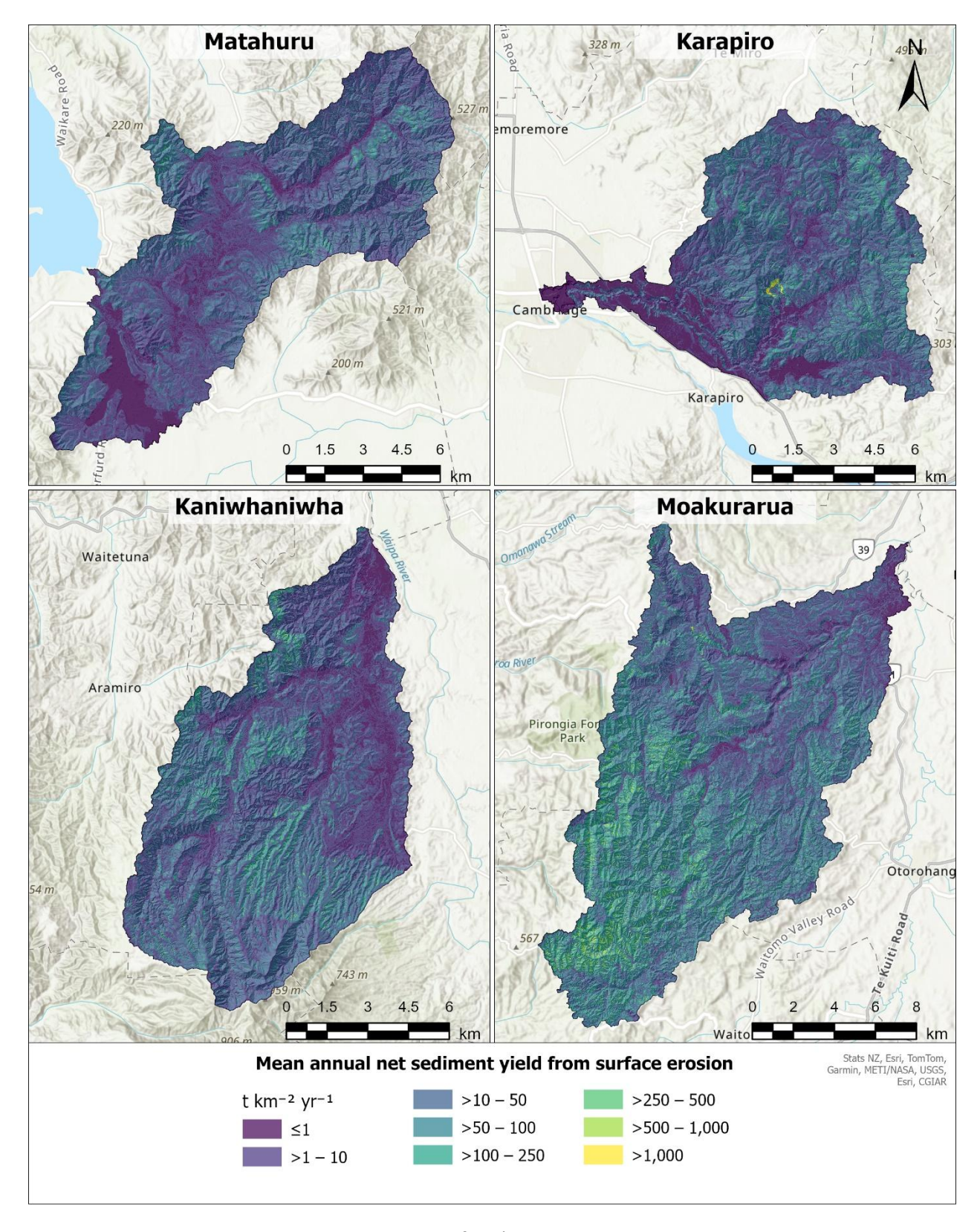


Figure 6. Mean annual net sediment yield (t km⁻² yr⁻¹) from surface erosion delivered to the stream network based on 2018 land cover from LCDB v5.0 and existing soil conservation works, displayed over the underlying hillshade layer. The sediment yields account for sediment trapping by riparian buffers, which is determined for each subwatershed and applied across all pixels within the subwatershed.

4.1.3 Riverbank erosion

The mean annual net sediment load from bank erosion equated to 3.8 kt yr⁻¹, 1.8 kt yr⁻¹, 0.85 kt yr⁻¹, and 0.50 kt yr⁻¹ for Moakurarua, Kaniwhaniwha, Matahuru, and Karapiro, respectively. This total net load compares with 1.6 kt yr⁻¹, 0.70 kt yr⁻¹, 0.33 kt yr⁻¹, and 0.22 kt yr⁻¹, respectively, based on the previous region wide SedNetNZ estimates from Vale & Smith (2024). Most of this increase in sediment load contribution from bank erosion was attributable to the increase in the length of the digital stream network (Table 1). This increase in network length largely reflects the improved representation of channel sinuosity based on the LiDAR-derived DEM as well as the difference in channel initiation threshold compared to the REC2 digital network (Figure 2). Figure 7 shows the spatial pattern in predicted reach-averaged mean annual net sediment yields from bank erosion for the CEM catchments.

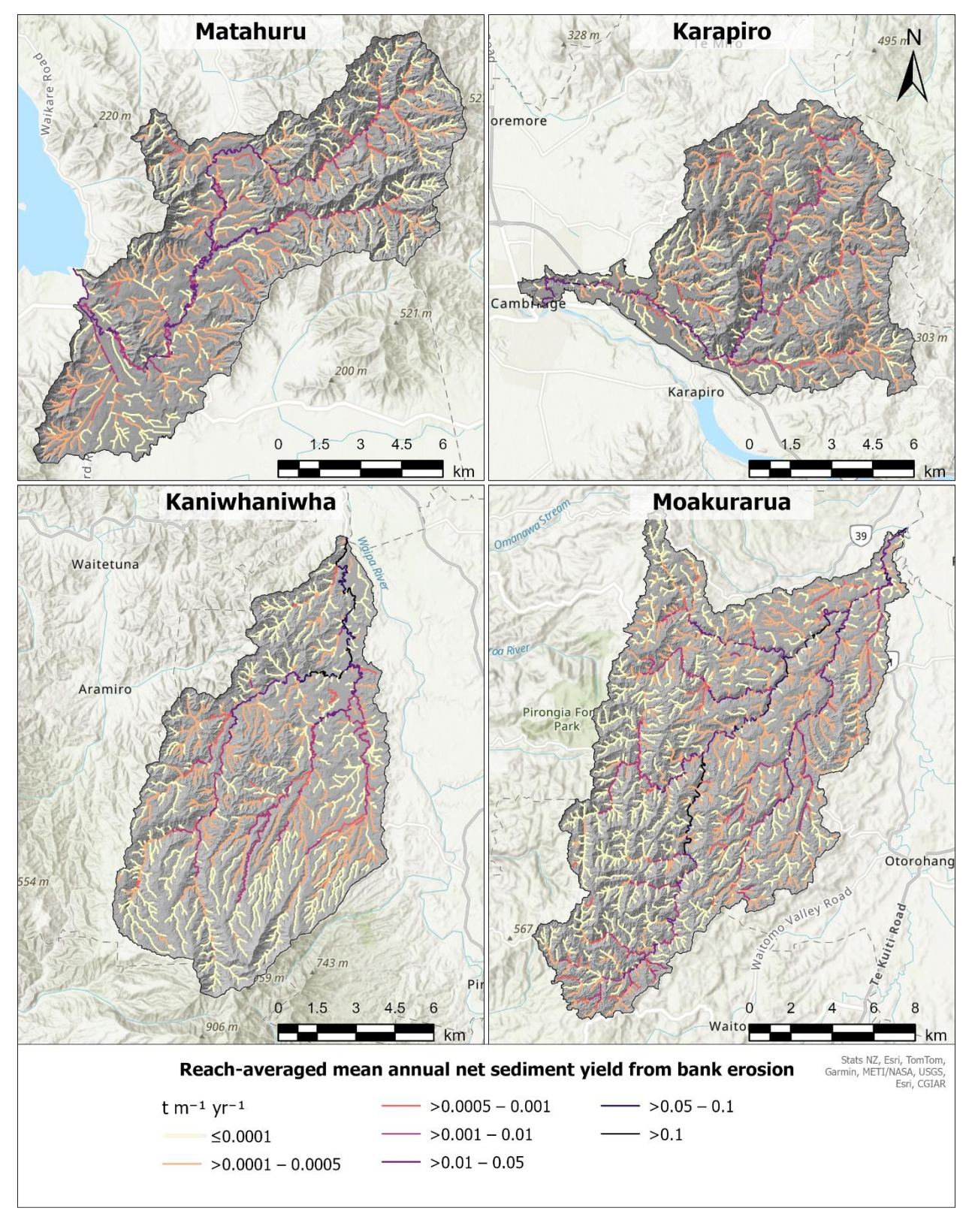


Figure 7. Predicted reach-averaged mean annual net bank sediment yield (t m⁻¹ yr⁻¹) per stream segment length for each segment in the LiDAR DEM-derived digital network.

4.1.4 Catchment suspended sediment budgets

Contemporary baseline (C2023)

Mean annual erosion loads, and net suspended sediment load delivered to the catchment outlet, as well as the erosion process contributions to suspended sediment loads in the LiDAR-based SedNetNZ sediment budgets are summarised for each CEM catchment in Table 9. Erosion load refers to the mean annual sediment load delivered to a stream segment from all erosion processes occurring in a subwatershed.

Figure 8 shows the mean annual net suspended sediment load per subwatershed, which is the load that accumulates downstream while accounting for losses of sediment into long-term storage in lakes and on floodplains. The net suspended sediment load delivered to the catchment outlet amounted to 33.4 kt yr⁻¹, 14.4 kt yr⁻¹, 13.2 kt yr⁻¹, and 6.6 kt yr⁻¹ for Moakurarua, Matahuru, Kaniwhaniwha, and Karapiro, respectively. Over a multi-decadal timescale, shallow landslides contribute an estimated 81% of the suspended sediment load in Matahuru, 56% in Kaniwhaniwha, 54% in Karapiro, and 42% in Moakurarua. Surface erosion accounts for 14%–46% across the CEM catchments, while riverbank erosion contributes 6%–13%.

Figure 9 shows the spatial pattern in mean annual net sediment yields (t km $^{-2}$ yr $^{-1}$) per subwatershed across each CEM catchment. The sediment yield was calculated as the sum of net sediment loads from each erosion process present within each subwatershed divided by the subwatershed area. This does not account for downstream storage of sediment in lakes and on floodplains. The largest sediment yields typically occur in areas of pastoral hill country on erodible, soft rock terrain as well as along sections of eroding river channel. Lower sediment yields occur in areas with woody vegetation cover or low slope. In a few cases, high yields (t km $^{-2}$ yr $^{-1}$) occur in subwatersheds with relatively low total erosion loads (t yr $^{-1}$) due to the very small areas of these subwatersheds (< 0.005 km 2).

Table 9. Summary of mean annual erosion load, mean annual net sediment load, and erosion process load contribution estimated for the contemporary baseline (C2023) for each CEM catchment using the LiDAR-based SedNetNZ model

CEM	Erosion load delivered to the	Mean annual net sediment load	Erosion load delivered to the stream network from each process ^a (kt yr ⁻¹ , %)							
catchment	stream network (kt yr ⁻¹)	delivered to end of catchment (kt yr ⁻¹)	Shallow landslide erosion	Earthflow erosion	Surface erosion	Riverbank erosion				
Kaniwhaniwha	13.8	13.2	7.8 56%	0.8 6%	3.4 25%	1.8 13%				
Karapiro	6.9	6.6	3.7 54%	- 0%	2.7 39%	0.5 7%				
Matahuru	15.1	14.4	12.2 81%	- 0%	2.1 14%	0.9 6%				
Moakurarua	34.9	33.4	14.6 42%	0.4 1%	16.2 46%	3.8 11%				

^a Gully-associated erosion loads, such as from gully erosion processes observed in the lower Karapiro, are captured by the surface and shallow landslide loads.

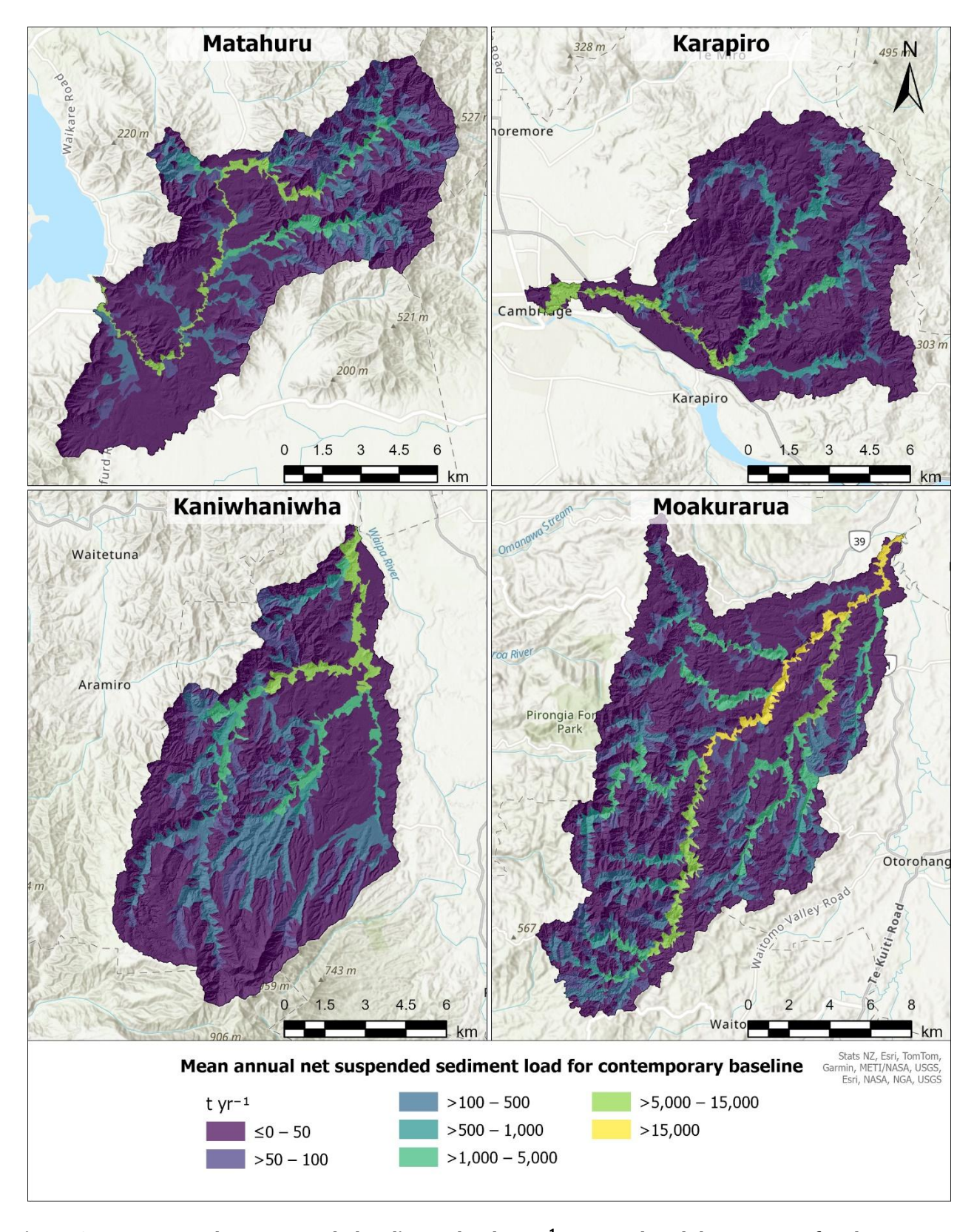


Figure 8. Mean annual net suspended sediment load (t yr⁻¹) accumulated downstream for the contemporary baseline (C2023) based on 2018 land cover from LCDB v5.0 and existing soil conservation works displayed for subwatersheds over the underlying hillshade layer.

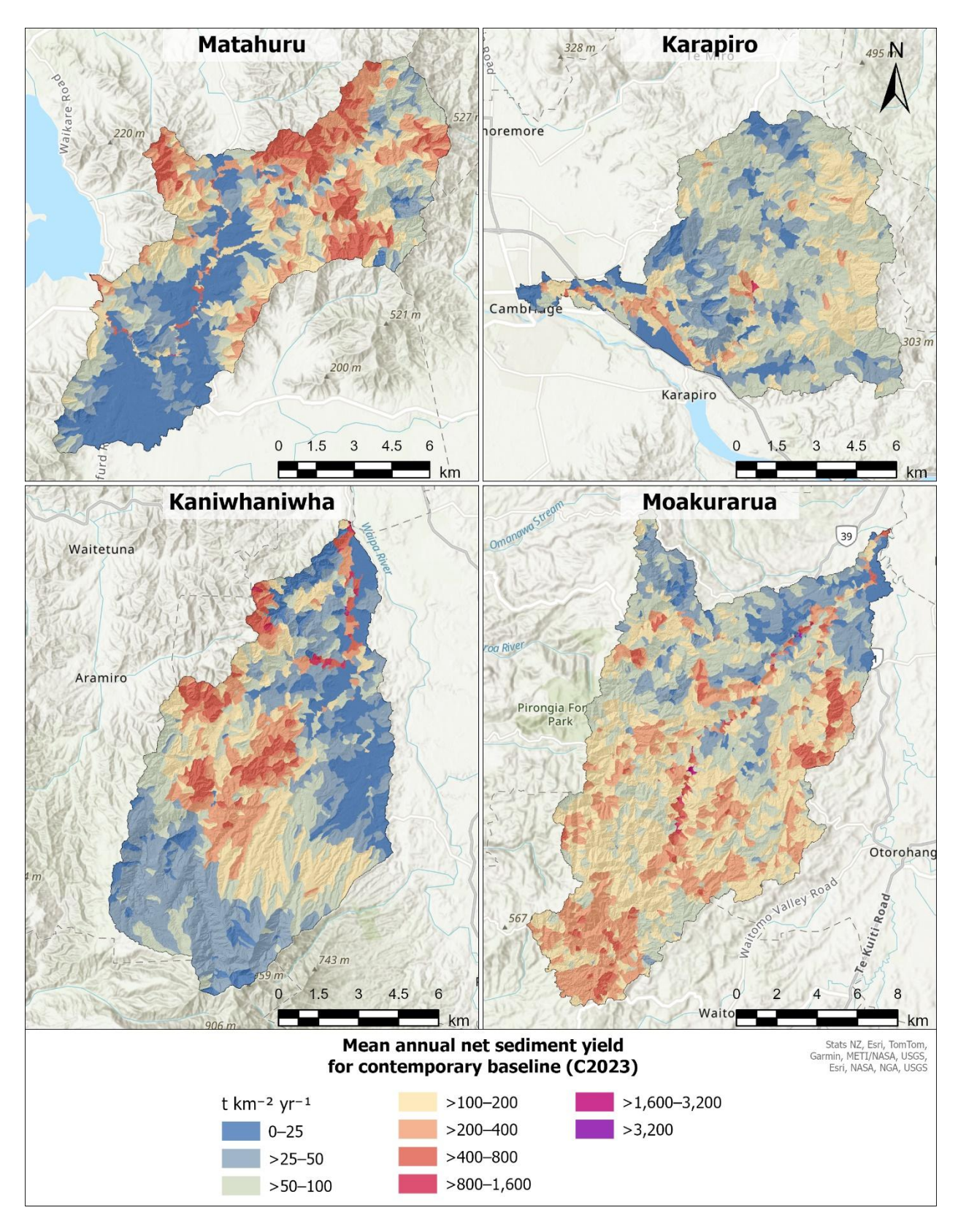


Figure 9. Mean annual net sediment yield (t km^{-2} y^{-1}) per subwatershed for the contemporary baseline (C2023) based on 2018 land cover from LCDB v5.0 and existing soil conservation works displayed over the underlying hillshade layer.

Combined mitigation scenarios

The future erosion mitigation scenarios used a 'ranked-watershed' approach to represent the implementation of erosion mitigation works (either afforestation/bush retirement or space-planted trees) on 20% to 100% of pastoral land based on slope thresholds (see Section 3.3.1). Erosion loads for each CEM catchment are presented in Table 10, and mean annual net sediment yields (t $\rm km^{-2}~yr^{-1}$) are shown in Figure 10 for the full implementation of the M1 scenario. Figure 11 and Figure 12 show the reductions in mean annual net sediment yield for 20%, 50%, and 100% implementation of the M1 scenarios.

Under the M1 scenario with 20% implementation, total erosion load decreases by 8%–14% relative to the contemporary baseline across all CEM catchments. A slightly larger reduction of 9%–16% is observed under the M2 scenario. With 50% implementation, erosion reductions increase to 13%–25% under M1 and 16%–29% under M2. Full implementation results in reductions of 21%–41% under M1 and of 23%–45% under M2 (Table 10).

The Matahuru experiences the largest proportional reductions, with 20% implementation decreasing total erosion by 14% and 16% under the M1 and M2 scenarios, respectively. These reductions increase to 41% and 45% under full implementation.

Table 10. Erosion loads (kt yr⁻¹) for each CEM catchment modelled under future erosion mitigation scenarios and showing % of implementation. M1 – M1 scenario (upper rows); M2 – M2 scenario (lower rows).

CEM (C2023: kt yr ⁻¹)	Erosion load per mitigation scenario and % implementation (kt yr ⁻¹)						Difference from contemporary baseline (C2023) (kt yr ⁻¹ , %)					
(ozozoz 111 y)		20%	30%	40%	50%	100%	20%	30%	40%	50%	100%	
Kaniwhaniwha	M1	12.4	12.0	11.8	11.5	10.5	-1.4 -10%	-1.8 -13%	-2.0 -15%	-2.3 -17%	-3.3 -24%	
(13.8)	M2	12.2	11.8	11.6	11.3	10.2	-1.6 -11%	-2.0 -14%	-2.2 -15.9%	-2.5 -18%	-3.6 -26%	
Karapiro	M1	6.4	6.2	6.1	6.0	5.5	-0.6 -8%	-0.7 -10%	-0.8 -12%	-0.9 -13%	-1.4 -21%	
(6.9)	M2	6.3	6.2	6.0	5.9	5.3	-0.6 -9%	-0.8 -11%	-0.9 -13%	-1.1 -16%	-1.6 -23%	
Matahuru	M1	13.0	12.5	12.0	11.4	8.9	-2.1 -14%	-2.7 -18%	-3.2 -21%	-3.8 -25%	-6.2 -41%	
(15.1)	M2	12.7	12.1	11.5	10.8	8.3	-2.4 -16%	-3.0 -20%	-3.6 -24%	-4.3 -29%	-6.9 -45%	
Moakurarua	M1	31.7	30.9	30.3	29.6	26.4	-3.2 -9%	-4.0 -12%	-4.6 -13%	-5.3 -15%	-8.5 -24%	
(34.9)	M2	31.2	30.4	29.5	28.6	25.3	-3.8 -11%	-4.5 -13%	-5.4 -16%	-6.3 -18%	-9.6 -28%	

The Kaniwhaniwha and Moakurarua show similar reductions in erosion load. For 20% implementation, reductions are 10% and 11% in Kaniwhaniwha and 9% and 11% in Moakurarua under M1 and M2, respectively. With full implementation, reductions increase to 24% and 26% in Kaniwhaniwha and 24% and 28% in Moakurarua, under M1 and M2, respectively. Moakurarua shows the largest total load reductions of 8.5 and 9.6 kt yr⁻¹ at full implementation under M1 and M2, respectively. This reflects the larger catchment size and sediment load in this catchment.

The smallest proportional reductions occur in the Karapiro, with 20% implementation producing decreases of 8% and 9% under M1 and M2, increasing to 21% and 23% under full implementation. Karapiro, the smallest CEM catchment, has the smallest total load reductions of 1.4 and 1.6 kt yr⁻¹ being achieved at full implementation under M1 and M2, respectively (Table 10).

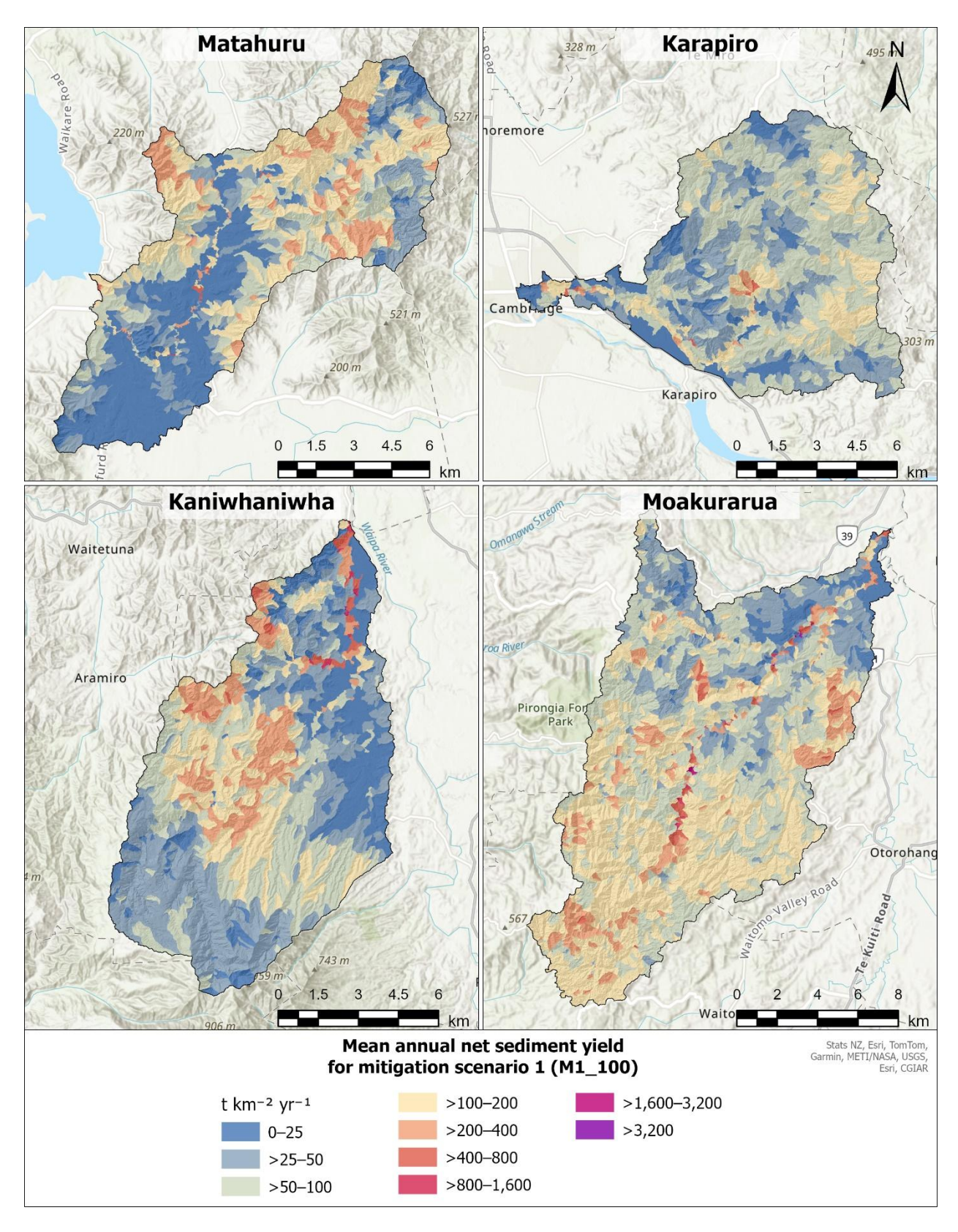


Figure 10. Mean annual net sediment yield (t km⁻² y⁻¹) per subwatershed for full implementation of the M1 scenario using the LiDAR-based digital network displayed over the underlying hillshade layer.

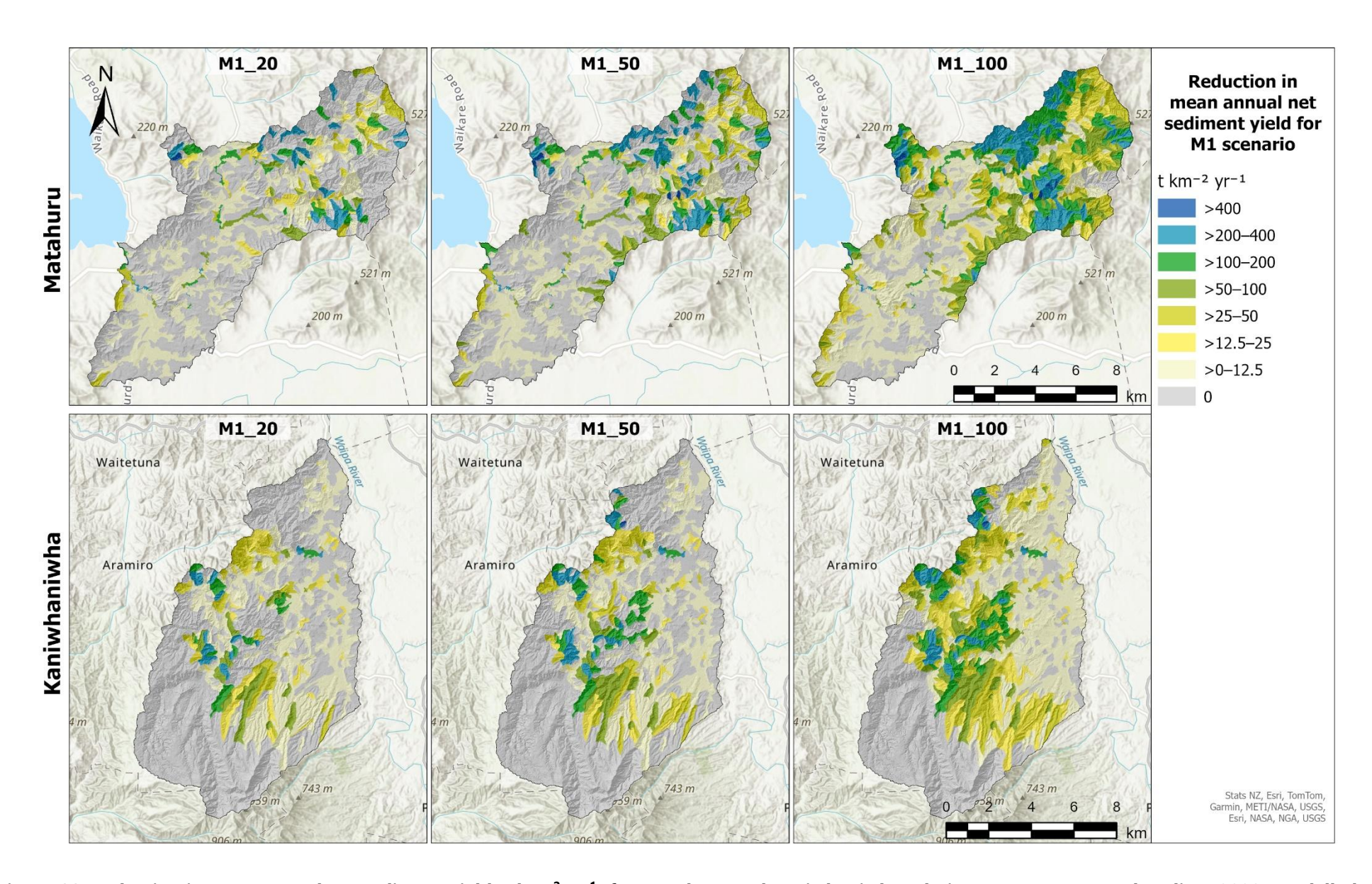


Figure 11. Reduction in mean annual net sediment yield (t km⁻² yr⁻¹) for Matahuru and Kaniwhaniwha relative to contemporary baseline (2023) modelled for the M1 erosion mitigation scenario at 20%, 50% and 100% implementation (labelled as M1_20, M1_50, and M1_100).

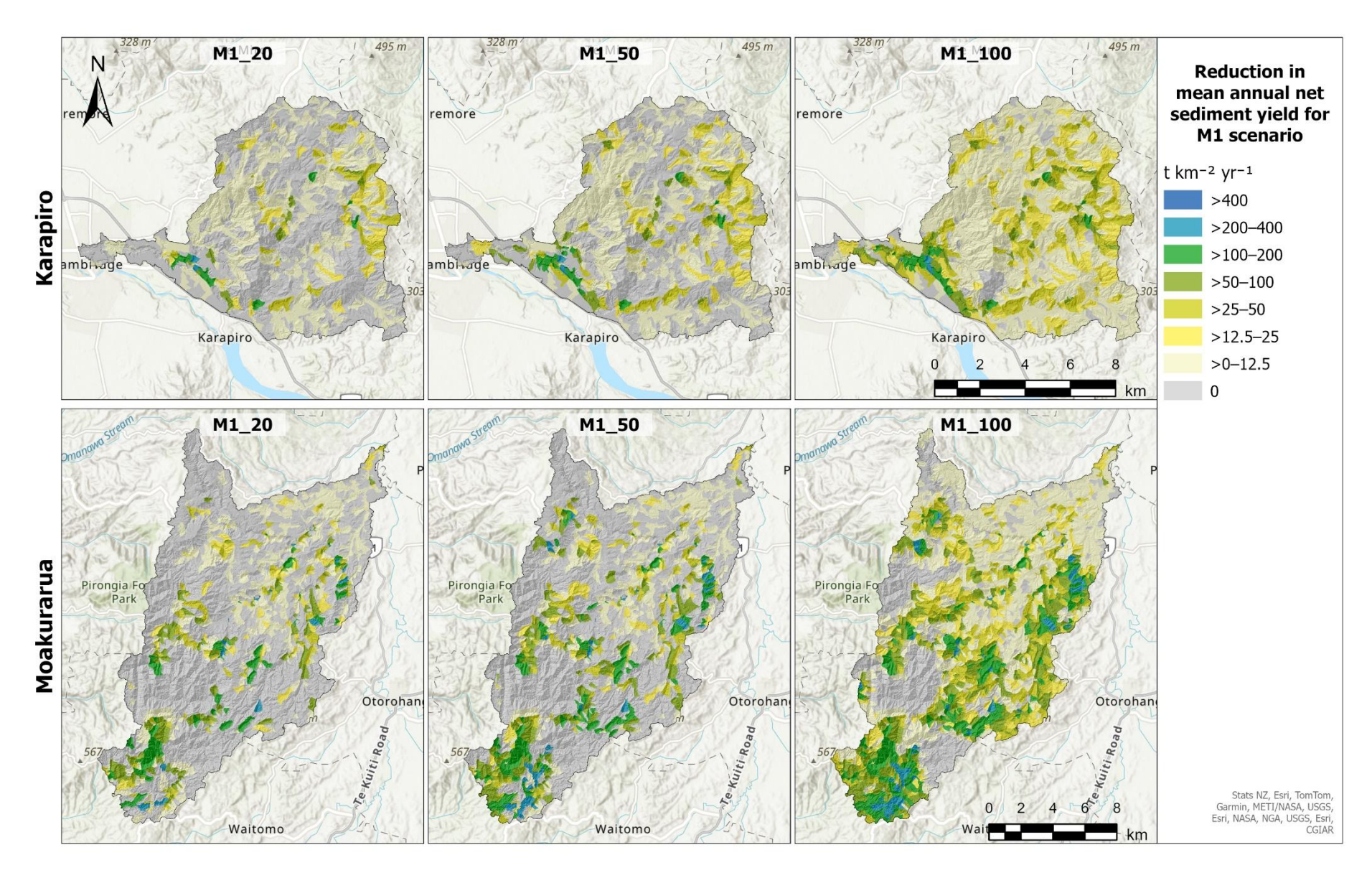


Figure 12. Reduction in mean annual net sediment yield (t km⁻² yr⁻¹) for Karapiro and Moakurarua relative to contemporary baseline (2023) modelled for the M1 erosion mitigation scenario at 20%, 50% and 100% implementation (labelled as M1_20, M1_50, and M1_100).

Individual mitigation scenarios

Under individual erosion mitigation scenarios, space-planted trees would achieve the largest proportional sediment reductions under the M1 scenario, while afforestation and bush retirement provide the greatest reductions under M2, across all CEM catchments (Table 11). This reflects the greater extent of space-planted trees relative to afforestation and bush retirement in M1, whereas in M2, the extent of afforestation and bush retirement is larger than space-planted trees.

The largest sediment load reductions from afforestation and bush retirement occur in Matahuru, decreasing by 16% and 32% under M1 and M2, respectively. Moakurarua shows reductions of 12% under M1 and 20% under M2, while Kaniwhaniwha sees reductions of 11% and 18% under M1 and M2, respectively. Karapiro shows the smallest reductions of 7% under M1 and 14% under M2 (Table 11).

Sediment load reductions from space-planted trees are largest in Matahuru (24% under M1 and 12% under M2) and Kaniwhaniwha (17% under M1 and 12% under M2). In Moakurarua, reductions are more moderate (12% under M1 and 7% under M2), while Karapiro sees smaller reductions (12% under M1 and 7% under M2). Riparian stock-exclusion fencing produced the smallest load reductions of the three mitigation types, with the largest reduction occurring in Kaniwhaniwha (7%) and Moakurarua (5%), followed by Matahuru (4%) and Karapiro (4%) (Table 11).

Table 11. Mean annual erosion loads (kt yr⁻¹) modelled for individual erosion mitigation types for each CEM catchment. M1 – M1 scenario (upper rows); M2 – M2 scenario (lower rows).

СЕМ	Me		ion load for each igation type (kt yr ⁻¹)		Difference from contemporary baseline (C2023) (kt yr ⁻¹ , %)				
(C2023: kt yr ⁻¹)		Afforestation & bush retirement	Space-planted trees	Riparian fencing	Afforestation & bush retirement	Space-planted trees	Riparian fencing		
Kaniwhaniwha	M1	12.4	11.4	12.9	-1.4 -10%	-2.4 -17%	-0.9 -7%		
(13.8)	M2	11.3	12.2	12.9	-2.5 -18%	-1.6 -12%	-0.9 -7%		
Karapiro	M1	6.4	6.1	6.6	-0.5 -7%	-0.8 -12%	-0.3 -4%		
(6.9)	M2	5.9	6.5	6.6	-1.0 -14%	-0.5 -7%	-0.3 -4%		
Matahuru	M1	12.7	11.5	14.5	-2.4 -16%	-3.6 -24%	-0.6 -4%		
(15.1)	M2	10.3	13.3	14.5	-4.8 -32%	−1.8 −12%	-0.6 -4%		
Moakurarua	M1	30.9	30.8	33.1	-4.1 -12%	-4.1 -12%	-1.9 -5%		
(34.9)	M2	27.9	32.7	33.1	-7.0 -20%	-2.3 -7%	-1.9 -5%		

4.2 Sediment load reductions required to meet NPS-FM visual clarity attribute bands

Suspended sediment load reductions required to achieve the NPS-FM 2020 suspended fine sediment attribute bands were modelled to determine proportional reductions at SOE sites within the CEM catchments for both the contemporary baseline (C2023) and future mitigation scenarios.

Baseline attribute states for each SOE site were determined using the median measured visual clarity based on data provided by WRC (see Section 3.4). Table 12 shows the proportional reductions (%) in suspended sediment load required to achieve the NPS-FM attribute bands and the NBL at each SOE site for the contemporary baseline. Table 13 and Table 14 show the proportional reductions in load that are still required after implementing the future combined and individual mitigation scenarios, respectively.

All SOE sites have a D attribute band base state and require reductions in sediment load to achieve the NBL for the contemporary baseline. Required reductions are 62% for Matahuru, 55% for Kaniwhaniwha, 51% for Karapiro, and 36% for Moakurarua. Achieving the B and A attribute bands would require reductions ranging from 47%–72% and 56%–78%, respectively (Table 12).

Table 12. Proportional reductions (%) in suspended sediment load required to achieve NPS-FM (2020) attribute bands (B and A) and the NBL (band C) at SOE monitoring sites under the contemporary baseline

		Base	Contempo	rary baselin	e (C2023)
Site name	Site ID	attribute state	C (NBL)	B %	A %
Kaniwhaniwha Stm at Wright Rd	222_16	D	55%	63%	69%
Karapiro Stm at Hickey Rd Bridge – Cambridge	230_5	D	51%	59%	66%
Matahuru Stm at Waiterimu Road Below Confluence	516_5	D	62%	72%	78%
Moakurarua Stm at Warratah Farm Bridge	553_12	D	36%	47%	56%

Both M1 and M2 scenarios show similar reductions in load are still required after scenario implementation to achieve the NBL and A and B attribute bands, although M2 needs slightly lower reductions. Under these scenarios and at 20% implementation, achieving the NBL requires further reductions in load of 55%–56% for Matahuru, 48% for Kaniwhaniwha, 46%–47% for Karapiro, and 28%–30% for Moakurarua. With full implementation, required reductions decrease to 32%–36% for Matahuru, 37%–39% for Kaniwhaniwha, 38%–40% for Karapiro, and 12%–15% for Moakurarua. At full implementation, neither M1 nor M2 scenarios achieve the NBL at any SOE site (Table 13).

There is a similar pattern for reductions in load required to achieve B and A attribute bands. Achieving attribute band A at 20% implementation requires reductions of 74%–75% for Matahuru, 64%–65% for Kaniwhaniwha, 63% for Karapiro, and 51%–52% for Moakurarua. With full implementation, required reductions decrease to 61%–63% for Matahuru, 57–58% for Kaniwhaniwha, 58%–59% for Karapiro, and 39%–42% for Moakurarua (Table 14).

Table 13. Proportional reductions (%) in suspended sediment load still required to achieve NPS-FM (2020) attribute bands (C, B or A) and the NBL at SOE monitoring sites following implementation of the combined erosion mitigation scenarios (M1 and M2) which includes all mitigation types.

					Propo	ortiona	al reduc	tions (load stil	-		or each	mitiga	tion s	cenario	and	
Scenario	Site name	Site ID	Base attribute	20%		30%		40%			50%			•	100%			
Scenario	Site name	Site ID	state	C (NBL) %	В %	A %	C (NBL) %	B %	A %	C (NBL) %	В %	A %	C (NBL) %	В %	A %	C (NBL) %	B %	A %
	Kaniwhaniwha Stm at Wright Rd	222_16	D	48%	57%	65%	47%	56%	64%	46%	55%	63%	45%	54%	62%	39%	50%	58%
Mitigation	Karapiro Stm at Hickey Rd Bridge – Cambridge	230_5	D	47%	56%	63%	46%	55%	63%	45%	55%	62%	44%	54%	62%	40%	50%	59%
(M1)	Matahuru Stm at Waiterimu Road Below Confluence	516_5	D	56%	67%	75%	54%	66%	74%	53%	65%	73%	50%	63%	71%	36%	52%	63%
	Moakurarua Stm at Warratah Farm Bridge	553_12	D	30%	42%	52%	28%	40%	50%	26%	39%	49%	24%	38%	48%	15%	30%	42%
	Kaniwhaniwha Stm at Wright Rd	222_16	D	48%	57%	64%	46%	55%	63%	45%	55%	62%	44%	53%	61%	37%	48%	57%
Mitigation scenario 2	Karapiro Stm at Hickey Rd Bridge – Cambridge	230_5	D	46%	56%	63%	45%	55%	62%	45%	54%	62%	43%	53%	61%	38%	49%	58%
(M2)	Matahuru Stm at Waiterimu Road Below Confluence	516_5	D	55%	67%	74%	53%	65%	73%	51%	63%	72%	48%	61%	70%	32%	49%	61%
	Moakurarua Stm at Warratah Farm Bridge	553_12	D	28%	41%	51%	27%	39%	50%	24%	38%	48%	22%	36%	46%	12%	27%	39%

Table 14. Proportional reductions (%) in suspended sediment load still required to achieve NPS-FM (2020) attribute bands (C, B or A) and the NBL at SOE monitoring sites following implementation of individual erosion mitigation types under M1 and M2 scenarios for each CEM catchment

					•		ıctions (%) n type, scei		•			
Scenario	Site name	Site	Base te attribute state		station & etirement		Space-planted trees			Riparian fencing and planting		
				C (NBL) %	B %	A %	C (NBL) %	B %	A %	C (NBL) %	B %	A %
	Kaniwhaniwha Stm at Wright Rd	222_16	D	49%	58%	65%	44%	54%	62%	51%	59%	66%
Mitigation	Karapiro Stm at Hickey Rd Bridge – Cambridge	230_5	D	48%	57%	64%	44%	54%	62%	48%	57%	64%
scenario 1 (M1)	Matahuru Stm at Waiterimu Road Below Confluence	516_5	D	55%	67%	74%	51%	63%	72%	61%	71%	78%
	Moakurarua Stm at Warratah Farm Bridge	553_12	D	27%	40%	50%	28%	41%	50%	32%	44%	54%
	Kaniwhaniwha Stm at Wright Rd	222_16	D	44%	54%	62%	48%	57%	64%	51%	59%	66%
Mitigation	Karapiro Stm at Hickey Rd Bridge – Cambridge	230_5	D	44%	54%	62%	47%	56%	64%	48%	57%	64%
scenario 2 (M2)	Matahuru Stm at Waiterimu Road Below Confluence	516_5	D	45%	59%	68%	57%	68%	76%	61%	71%	78%
	Moakurarua Stm at Warratah Farm Bridge	553_12	D	20%	34%	45%	32%	44%	53%	32%	44%	54%

4.3 Model evaluation and limitations

4.3.1 SedNetNZ model evaluation

SedNetNZ is designed to predict spatial patterns in erosion and suspended sediment load on a mean annual basis for periods spanning several decades. It is difficult to quantify model performance over such time scales other than through comparison with measurements of suspended sediment loads, which has been the main form of SedNetNZ model evaluation (Basher et al. 2018). Longer-term suspended sediment load data are often unavailable. However, rivers have been monitored in the Waikato region and the resulting suspended sediment concentration (SSC) and discharge (Q) data used to estimate mean annual suspended sediment loads via SSC-Q rating curve methods (e.g. Hicks et al. 2019). River monitoring sites are located in the lower reaches of the CEM catchments. Flow and sediment sampling monitoring periods span 8–18 years, except for in Karapiro, which has only 1 year of data (Table 15). While the monitoring sites are in the lower reaches of the CEM catchments, they are not end-of-catchment loads and exclude some contributions from erosion occurring downstream from the sites.

Table 15. Comparison of SSC-Q rating curve estimates of mean annual suspended sediment load versus LiDAR-based SedNetNZ model predictions

River monitoring site name	Catchment area (km²)	Flow measurement period	Sediment sampling period	WRC SSC-Q sediment loads ^a (kt yr ⁻¹)	Previous regionwide non- LiDAR SedNetNZ (Vale & Smith, 2024) (kt yr ⁻¹)	CEM catchment LiDAR-based SedNetNZ (present report) (kt yr ⁻¹)
Kaniwhaniwha at Wright Rd (222_16)	103	2015 – 2024	2016 – 2024	9.9	10.0	11.4
Karapiro at Horotiu Rd Bridge (SH1) (230_41)	82	2023-2024	2023-2024	7.6	10.0	6.5
Matahuru at Myjers (516_22)	83	2006 – 2024	2006 – 2024	17.4	14.3	13.8
Moakurarua at Warratah Farm Br (553_12)	206	2015 – 2024	2015 – 2024	36.9	40.6	30.8

^aSSC-Q rating curve estimates incorporate TSS-SSC corrections to refine sediment load estimates, except for Matahuru, where uncorrected values are reported due to an insufficient number of samples to establish a reliable correction.

While caution is needed when comparing the SSC-Q estimated loads with model predictions that are based on a multi-decadal timescale, there is general agreement between modelled loads and rating curve estimates (Table 15). This comparison is indicative only, given the limited number of sites we had for comparing model predictions with estimates, and the inherent limitations of rating curve-based estimates (Asselman 2000; Vercruysse et al. 2017) – particularly related to the monitoring period they represent. Suspended sediment and flow data extend back to 2006 in Matahuru, 2015 in Kaniwhaniwha and Moakurarua, and 2023 in Karapiro. Longer records may reflect land cover and erosion control works (e.g. tree planting) that differ from the contemporary baseline state modelled. This is especially relevant for soil conservation efforts and riparian fencing

incorporated into the model based on the most recent data that may reduce sediment loads compared to historical estimates from river monitoring.

However, rating curve-based estimates that span multi-decadal periods have an averaging effect, which is important when comparing with SedNetNZ load predictions. In contrast, shorter records (e.g. Karapiro) are more likely to be influenced by the specific rainfall, river flow, and sediment transport conditions observed during those intervals. For instance, short monitoring intervals may not capture the impact of landslide-triggering events that occur episodically and contribute significant quantities of sediment to the stream network.

Comparison with previous modelling

The LiDAR-based SedNetNZ load estimates are generally similar to previous region-wide modelling (Vale & Smith 2024) albeit slightly lower at all river monitoring sites except in Kaniwhaniwha, where the loads are marginally higher (Table 15). These differences reflect differences in the extent of modelled soil conservation works, such as riparian fencing mentioned above. Thay also reflect inherent variations in erosion process representation (and resulting erosion process loads) within the LiDAR DEM-based sub-models, where more substantial changes to individual erosion process loads are observed.

Evaluating modelled erosion process contributions to sediment loads is challenging as we lack data to apportion sediment loads from gauged river monitoring sites to individual erosion processes averaged over multi-decadal timescales. The LiDAR-based SedNetNZ modelling shows differences in process contributions compared to previous region-wide modelling, with variations observed across all CEM catchments. In general, there is a decrease in the relative contribution of shallow landslides and an increase in surface and riverbank erosion contribution (Table 16). However, these shifts do not always correspond to significant changes in absolute sediment loads.

The contribution of shallow landslides to the sediment load decreases to 81% in Matahuru, 56% in Kaniwhaniwha, 54% in Karapiro, and 42% in Moakurarua, compared to 93%, 71%, 85%, and 65%, respectively, in the previous region-wide modelling (Table 16). Despite this reduction in relative contribution, the absolute shallow landslide sediment loads remain relatively similar in Kaniwhaniwha (7.8 vs 7.9 kt yr⁻¹) and Matahuru (12.2 vs 15.2 kt yr⁻¹). In contrast, Karapiro (3.7 vs. 8.5 kt yr⁻¹) and Moakurarua (14.6 vs. 28.0 kt yr⁻¹) show larger reductions (Table 16). Regardless of these changes, shallow landslides remain the dominant source of sediment across the CEM catchments, except for the Moakurarua where the contribution from shallow landslides (42%) is now marginally lower than from surface erosion (46%).

Surface erosion increases to between 14% and 46% across the CEMs, compared to 5%–30% in the previous modelling. This corresponds to an approximate doubling of surface erosion loads in Kaniwhaniwha, Karapiro, and Matahuru, with loads increasing from 0.8–1.8 kt yr⁻¹ to 2.1–3.4 kt yr⁻¹. In Moakurarua, the increase is smaller, with surface erosion now contributing 16.2 kt yr⁻¹, compared to 12.8 kt yr⁻¹ previously. Similarly, riverbank erosion also increases, now contributing 6%–13% across the CEM catchments, compared to 2%–6% in the previous modelling which is mostly attributed to the increase in the length of the digital stream network (Table 1). This results in an approximately twofold increase in riverbank erosion loads, with values rising to 0.5–3.8 kt yr⁻¹, compared to 0.2–1.6 kt yr⁻¹ in earlier estimates (Table 16).

Table 16. Comparison of erosion process loads between the LiDAR-based SedNetNZ and the previous region-wide non-LiDAR SedNetNZ results for each CEM catchment

		Total erosi	on load deli	vered to the (kt yr	stream netw ^{–1} , %)	ork from eac	h process ^a	
		LiDAR-based (present			Previous	regionwide r (Vale & Sn		SedNetNZ
CEM catchment	Shallow landslide erosion	Earthflow erosion	Surface erosion	Riverbank erosion	Shallow landslide erosion	Earthflow erosion	Surface erosion	Riverbank erosion
Kaniwhaniwha	7.8	0.8	3.4	1.8	7.9	0.8	1.8	0.7
	56%	6%	25%	13%	71%	7%	16%	6%
Karapiro	3.7	-	2.7	0.5	8.5	-	1.2	0.2
	54%	0%	39%	7%	85%	0%	12%	2%
Matahuru	12.2	-	2.1	0.9	15.2	-	0.8	0.3
	81%	0%	14%	6%	93%	0%	5%	2%
Moakurarua	14.6	0.4	16.2	3.8	28.0	0.4	12.8	1.6
	42%	1%	46%	11%	65%	1%	30%	4%

^a Gully-associated sediment loads, such as from gully processes observed in the lower Karapiro, are captured by the surface and shallow landslide loads.

The LiDAR-based SedNetNZ modelling provides a more refined representation of erosion processes compared to previous region-wide modelling. Differences in estimated process contributions are primarily driven by the higher-resolution LiDAR-derived terrain data, which improves the representation of topographic controls on erosion, as well as improvements in the sub-models that adopt data-driven approaches using recently expanded data sets for model calibration. The observed decrease in the relative contribution of shallow landslides and the corresponding increase in surface and riverbank erosion reflect improvements in how these erosion processes are captured, particularly in relation to the spatial variability within individual catchments, which is more challenging to represent using the lower resolution terrain data that underpins the non-LiDAR regional-scale modelling.

At a subwatershed scale, erosion processes exhibit greater variability, especially in lowland areas, where riverbank erosion can be an important sediment source. The LiDAR-based approach better represents finer-scale variations, improving the ability to distinguish between erosion processes that may be underestimated or overgeneralised in region-wide assessments. This increased spatial precision strengthens the model's capacity to represent contemporary sediment budgets and supports its application in targeting erosion mitigations for improved sediment management.

We outline some specific limitations in terms of each modelling component below. Model outputs should be interpreted in the context of these limitations.

4.3.2 Model limitations

Limited empirical data presents an ongoing challenge in modelling erosion processes, particularly across New Zealand's diverse erosion terrains. This scarcity of data means model parameterisation must draw from the available data in combination with expert judgment when developing representations of erosion processes and mitigation effectiveness. While the LiDAR-based

SedNetNZ model offers significant improvements in erosion process representation, certain limitations remain due to data constraints and inherent modelling assumptions.

Erosion process representation

The surface erosion component of the LiDAR-based model was updated to improve representation of slope length and steepness to better represent the effect of topography on the size of convergent upslope areas contributing overland flow and surface erosion, following Smith, Herzig et al. (2019). One of the primary limitations in the surface erosion component continue to relate to the calculation of the \mathcal{C} and \mathcal{K} factors in RUSLE, and the availability of high-resolution input data. Further acquisition of higher-resolution soils data for the Waikato region, such as S-map, may improve estimates of surface erosion in future.

We introduced a new stocking density-adjusted *K* factor into the surface erosion sub-model to account for the effects of livestock treading and grazing on surface erosion. This approach required several parameters, including grazing intensity and stock type, soil moisture, clay content, soil susceptibility, and grazing history and duration (Donovan & Monaghan 2021). Many of these parameters exhibit both inter-annual variability and longer-term changes in response to land use and farming practices. However, due to the absence of suitable spatial or long-term data, we had to make assumptions for use in a multi-decadal sediment budget model. As a result, our model does not capture the inter-annual variability that is likely to occur.

Evaluating model performance over the multi-decadal timescale is challenging. However, Donovan & Monaghan (2021) reported good agreement between modelled and measured rates of soil loss at both catchment and farm scales, providing a useful basis for assessing the sensitivity of the adjustment to specific parameters. Based on the relationship curves in Figure 2 of Donovan & Monaghan (2021), soil damage appears to be most sensitive to stock type, grazing intensity, and clay content. We used local stock unit densities provided by WRC, derived from AgriBase®, to determine stock type and grazing density. While these data are temporally static, they offer the best available spatial representation at the catchment scale. In contrast, data for soil moisture, grazing history, and duration were unavailable, so we relied on approximated values from Donovan & Monaghan (2021). However, soil damage appears to be less sensitive to these parameters.

Comparing adjusted and non-adjusted surface erosion loads shows that incorporating the stocking density-adjusted K factor increases the surface erosion load by 2%–3% in Moakurarua, Karapiro, and Kaniwhaniwha, and by 10% in Matahuru. The overall impact on modelled catchment loads is therefore limited (0.8%–1.2% of total erosion load across the CEM catchments), although may be significant in specific subwatersheds. This is because the highest stock densities – and therefore the most significant soil damage – tend to occur on lower-slope pastoral land, where surface erosion sediment yields are relatively low compared to steeper hill country.

Shallow landslides are initiated by storm events over a triggering threshold. This means the landslide load in any given year can vary significantly from the mean annual landslide load. This inter-annual variability in landslide occurrence is not represented in SedNetNZ. Instead, the storm-triggered shallow landslide contribution to the sediment load is averaged over a multi-decadal timescale as described in Section 3.2.1.

Landslide depth was approximated to a constant 1 m; however, actual depths can vary significantly. For example, Phillips et al. (2021) reported typical depths of up to 2 m, while Page et al. (1994) observed scar depths ranging from 0.13 to 3.9 m, with an average of 0.89 m. Betts et al. (2017) reported depths in various materials, including weakly indurated sandstone (0.2–1.6 m; mean 0.69 \pm 0.05 m), moderately indurated sandstone (0.3–1.4 m; mean 0.74 \pm 0.05 m), and mudstone (0.3–3.0 m; mean 1.01 \pm 0.07 m). Although informative, these data are limited, and we currently lack sufficient data to adequately represent this spatial variation in landslide depths within the model.

Earthflow and gully erosion are represented in SedNetNZ using a spatial averaging approach based on the estimated presence and spatial extent of these erosion features in the Erosion Terrains layer (Dymond et al. 2016), which has not changed in the LiDAR-based version of SedNetNZ. While this allows for region-wide representation, it introduces uncertainties at the subwatershed level and it is possible that earthflow and gully erosion may be represented in subwatersheds that do not contain these features or may not be represented where they are present, especially when using the higher resolution digital stream subwatershed layer derived from the 5 m DEM. Given their limited spatial extent, aerial imagery was previously used in the region-wide modelling (Vale & Smith 2024) to evaluate selected catchments. Adjustments were then made to the Erosion Terrain layers if there was limited evidence of significant active gully erosion at the resolution of the Erosion Terrain features, as well as with a comparison of modelled sediment loads with load estimates derived from SSC-Q rating curves.

This Erosion Terrain layer was used for the CEM catchments resulting in a very limited representation of earthflows and no mapped presence of gullies. While this means that gully-associated sediment loads are not explicitly modelled, such as those in the lower Karapiro, sediment load contributions are captured via representation of the surface and shallow landslide erosion processes occurring within these areas. This approach enables better representation of the spatial patterns in sediment loads at higher resolution than can be achieved using the Erosion Terrains, as can be seen in the modelled shallow landslide and surface erosion yields for Karapiro in Figure 5 and Figure 6.

Riverbank erosion modelling in SedNetNZ was improved through use of a much larger data set on bank migration rates for model calibration and LiDAR-derived estimates of bank height, which replaces earlier reliance on a simple regional discharge-bank height relationship. Access to high-resolution spatial data on riparian woody vegetation remains a key requirement for modelling bank erosion. For this reason, riparian woody vegetation cover is now derived directly from the LiDAR data at 1 m resolution, replacing use of the lower resolution (15 m) 'EcoSat Woody' layer (Dymond & Shepherd 2004). The LCDB is unsuitable for representing narrow strips of riparian vegetation due to its minimum mapping unit of 1 ha.

Erosion mitigation effectiveness

The reduction in sediment load from hillslope erosion processes is determined by the change in land cover related to each type of mitigation in each scenario. Effectiveness represents the capacity of an erosion mitigation to reduce sediment load once fully mature and is specific to each mitigation type. The effectiveness values we used in our modelling were based on simplifications of published data and assumed full effectiveness of mitigations once fully mature. However, a considerable range of effectiveness values for different erosion mitigations are reported in the

literature and real-world effectiveness can vary significantly. A comprehensive summary of erosion mitigation effectiveness is provided by Phillips et al. (2020).

We used an effectiveness value of 90% for the reduction of mass movement erosion following the conversion from pasture to permanent woody cover. This represents the reduction typically observed in New Zealand studies (Phillips et al. 2020). However, studies have reported ranges between 35% and 91%, with most indicating a 70%-90% reduction in landsliding under closed-canopy vegetation (such as indigenous forest, pines older than 8 years, or scrub) compared to pasture (e.g. DL Hicks 1989, 1990, 1991; Pain & Stephens 1990; Phillips et al. 1990; Marden et al. 1991; Bergin et al. 1993, 1995; Marden & Rowan 1993; Fransen & Brownlie 1995; Hancox & Wright 2005; Smith et al. 2023).

For the effectiveness of space-planted trees, we adopted a value of 70% based on data from Hawley and Dymond (1988) but supported more broadly by published studies. Most empirical data on the performance of space-planted trees for erosion control are based on individual or small groups of trees rather than hillslope-scale performance. Reported values range from 22% to 95% in various New Zealand studies (Phillips et al. 2020). The large range reflects the high dependence on successful establishment of the trees and subsequent maintenance to ensure their survival and effectiveness (see Marden & Phillips 2013). When plantings are adequately spaced (10 m) and well maintained, published reductions in shallow landsliding range from 70% to 95% (e.g. Hawley & Dymond 1988; Douglas et al. 2009, 2013; McIvor et al. 2015).

Determining the most appropriate effectiveness value for reductions in stream bank erosion arising from riparian fencing and stock-exclusion is challenging because of the limited studies available, with stream bank erosion one of the least understood erosion processes in New Zealand (Basher 2013). Bank erosion varies with stream order and scale (e.g. headwaters, lower reaches) and can occur through various processes, such as mass failure, stock trampling, and fluvial entrainment (Hughes 2016), making the impact of riparian management on bank erosion highly variable. Our effectiveness value falls within the 30%–90% range from published and unpublished sources (Owens et al. 1996; Williamson et al. 1996; Line et al. 2000; Meals & Hopkins 2002; McKergow et al. 2003, 2007; Monaghan & Quinn 2010; Phillips et al. 2020).

Riparian fencing estimate

The estimation of riparian fencing across the CEM catchments was derived from survey data provided by WRC from the CEM catchment riparian surveys conducted between 2020 and 2023. Relying on these surveys to estimate fencing extents introduces uncertainties, particularly when mapped onto the digital stream network. These uncertainties primarily stem from: a) limitations inherent in the survey data, including potential sample and observer biases and variability in data consistency across the catchments; and b) challenges in ensuring the spatial representativeness of average fencing estimates and their alignment with the digital stream network.

The WRC surveys employ a stratified sampling approach, creating distinct sub-groups to capture a range of variables, including land-use type, and stream order. A challenge arises in translating site-based fencing data to the catchment-wide digital stream network. Applying farm-type and stream-order-based average fencing proportions to represent catchment patterns introduces potential inaccuracies at specific stream segments. Also, while site surveys can determine farm types at specific locations, mapping these onto the digital stream network using AgriBase® farm

classifications provides only a coarse approximation of land use over time, potentially missing more varied land uses within farm type classifications.

Determining accurate fencing proportions is also complicated by the precision of the digital stream network. The digital network's sensitivity to the drainage area threshold for the initiation of first-order streams means its alignment with actual stream networks can vary across terrains. As a result, some first-order streams in the digital network may be perennial, ephemeral, or non-existent. We have addressed this issue by implementing a new digital stream network derived from the LiDAR 5 m DEM using a 5 ha initiation threshold. While some over- and underestimation of channel extent persists, the updated network represents a significant improvement in capturing the extent and planform of the actual stream network compared to the previous REC2 digital stream network.

Any overestimation of the contemporary riparian fencing extent limits the length of the remaining stream network available for further fencing and, consequently, the modelled future reduction in sediment load from additional riparian fencing. This limitation also affects the potential improvements in visual clarity and the ability to achieve NPS-FM 2020 attribute bands and the NBL. In contrast, underestimation of the contemporary fencing extent, will lead to potential overestimation of the levels of load reduction and clarity improvement achieved with future fencing.

Reductions required to meet visual clarity attribute bands

We estimated mean annual suspended sediment load reductions to achieve visual clarity and suspended fine sediment objectives using equations developed by Hicks et al. (2019) from simplifications in the relationships reported by Dymond et al. (2017). A key assumption for calculating required load reductions to meet objectives is that the relationship between suspended sediment load and the flow frequency distribution remain constant at a site. In reality, this relationship may change due to changes in catchment hydrology, leading to changes in the relationship between a given flow and suspended sediment load (Hicks et al. 2019).

Because data are not presently available to predict these changes, we have assumed that the associated relationships remain constant. This assumption is particularly important when modelling changes in visual clarity under different scenarios. Because these scenarios may significantly change the land cover and catchment hydrology, the relationship between visual clarity and sediment load may differ at an SOE site compared with the contemporary baseline (C2023).

We estimated the required load reductions using empirical models fitted to a national data set. This should result in the models being fitted to a wide range of catchment variables and therefore representing the variability across Waikato CEM catchments. Although sites from Waikato were used in the national data set (see Hicks et al. 2019), this approach may lead to under- or overestimation of required reductions at any one location.

5 Conclusions

This report describes work undertaken to model erosion and suspended sediment loads using the newly developed LiDAR-based version of SedNetNZ in four Waikato CEM catchments. The model predicted net suspended sediment load delivered to the catchment outlets, with estimates of 33.4 kt yr⁻¹, 14.4 kt yr⁻¹, 13.2 kt yr⁻¹, and 6.6 kt yr⁻¹ for Moakurarua, Matahuru, Kaniwhaniwha, and Karapiro, respectively, under contemporary conditions. Shallow landslides were mostly identified as the dominant sediment source, contributing 42%–81% of the load, while surface erosion accounted for 14%–46%, and riverbank erosion for 6%–13% across the catchments

Erosion mitigation scenarios (M1 and M2) comprising a combination of afforestation/bush retirement, spaced tree planting, and riparian fencing could reduce net sediment loads by 21%–45% under M1 and 23%–45% under M2. The Matahuru catchment showed the largest proportional reductions (of 41%–45%), while Moakurarua exhibited the greatest absolute reductions, with decreases of up to 9.6 kt yr⁻¹ under M2. Matahuru achieved the largest reductions from afforestation and bush retirement (16% under M1, 32% under M2), while Karapiro showed the smallest reductions (7% under M1, 14% under M2). Riparian fencing had the lowest proportional impact on sediment loads across all catchments.

Despite these reductions, none of the fully implemented mitigation scenarios achieved the NPS-FM (2020) NBL at any of the SOE sites. At full implementation of M1 and M2, further reductions of between 12% and 40% would still be needed to meet the NBL across the CEM catchments, with greater reductions (between 39% and 63%) required to achieve the A attribute band.

Modelled suspended sediment loads are generally consistent with SSC-Q rating curve estimates of loads from river monitoring sites, as well as with previous region-wide modelling, albeit being slightly lower; the exception is Kaniwhaniwha, where the load is marginally higher. These differences reflect variations in modelled soil conservation works, such as riparian fencing, and inherent changes in erosion process representation within the new erosion process sub-models.

Compared to previous region-wide modelling, there is a general decrease in the relative contribution of shallow landslides, accompanied by an increase in surface and riverbank erosion across all CEM catchments. While absolute sediment loads from shallow landslides remain similar in Kaniwhaniwha and Matahuru, larger reductions are seen in Karapiro and Moakurarua. Surface erosion contributions have approximately doubled in Kaniwhaniwha, Karapiro, and Matahuru, while riverbank erosion loads have approximately doubled for all CEM catchments, largely due to an increase in the length of the modelled digital stream network. These variations reflect differences in modelled soil conservation works and improvements in process representation enabled by higher-resolution LiDAR data.

6 Acknowledgements

We thank Waikato Regional Council for funding this work. We acknowledge staff from Waikato Regional Council, particularly Tim Norris and Haydon Jones, for discussions that defined the scope of work. We thank Andrew Neverman for reviewing the report.

7 References

- Asselman NEM 2000. Fitting and interpretation of sediment rating curves. Journal of Hydrology 234(3–4): 228–248. https://doi.org/10.1016/S0022-1694(00)00253-5
- AssureQuality. (2020). AgriBase®. https://www.asurequality.com/services/other-services/agribase/
- Basher L 2013. Erosion processes and their control in New Zealand: ecosystem services in New Zealand conditions and trends 2013. Lincoln, Manaaki Whenua Press. Pp. 363–374.
- Basher L, Spiekermann R, Dymond J, Herzig A, Ausseil A-G 2018. SedNetNZ, SLUI and contaminant generation. Part1: Sediment and water clarity. Manaaki Whenua Landcare Research Contract Report LC3135, prepared for Horizons Regional Council.
- Bergin DO, Kimberley MO, Marden M 1993. How soon does regenerating scrub control erosion? New Zealand Forestry 38(2): 38–40.
- Bergin DO, Kimberley MO, Marden M 1995. Protective value of regenerating tea-tree stands on erosion-prone hill country, East Coast, North Island, New Zealand. New Zealand Journal of Forestry Science 25: 3–19.
- Betts H, Basher L, Dymond J, Herzig A, Marden M, Phillips C 2017. Development of a landslide component for a sediment budget model. Environmental Modelling & Software 92: 28–39.
- Betts H, Spiekermann R, Dymond J 2017. SedNetNZ modelling of sediment sources and loads from the Western Waikato, Coromandel, Waihou-Piako and Taupo Water Management Zones, Waikato Region. Manaaki Whenua Landcare Research Contract Report LC2835, prepared for Waikato Regional Council
- Betts H, Smith HG, Neverman A, Tsyplenkov A, 2023. Wairoa shallow landslide and debris deposit mapping following storm events in March 2022. Landcare Research Contract Report LC4331 for Hawke's Bay Regional Council.
- Booker D, Hicks M 2013. Estimating wetted width and fish habitat areas across New Zealand's rivers: wetted widths estimation. NIWA client report CHC2013-075. Prepared for Department of Conservation.
- Brune GM 1953. Trap efficiency of reservoirs. Eos, Transactions American Geophysical Union 34(3): 407–418.
- Carter JV, Pan J, Rai SN, Galandiuk S 2016. ROC-ing along: evaluation and interpretation of receiver operating characteristic curves. Surgery 159: 1638–1645.
- Conoscenti C, Rotigliano E, Cama M, Caraballo-Arias N, Lombardo L, Agnesi V 2016. Exploring the effect of absence selection on landslide susceptibility models: a case study in Sicily, Italy. Geomorphology 261: 222–235.

- Curran-Cournane FC, McDowell R, Littlejohn R, Condron L 2011. Effects of cattle, sheep, and deer grazing on soil physical quality and losses of phosphorus and suspended sediment losses in surface runoff. Agriculture, Ecosystems & Environment 140: 264–272.
- Dairy Environment Leadership Group 2013. Sustainable Dairying: Water Accord: a commitment to New Zealand by the dairy sector. http://www.dairynz.co.nz/what-we-do/dairyindustry-strategy/
- De Rose R, Basher LR. 2011. Measurement of river bank and cliff erosion from sequential LiDAR and historical aerial photography. Geomorphology 126:132–147.
- Desmet P, Govers G 1996. A GIS procedure for automatically calculating the USLE LS factor on topographically complex landscape units. Journal of Soil and Water Conservation 51(5): 427–433.
- Donovan M 2022. Modelling soil loss from surface erosion at high resolution to better understand sources and drivers across land uses and catchments: a national-scale assessment of Aotearoa, New Zealand. Environmental Modelling & Software 147: 105228. https://doi.org/10.1016/j.envsoft.2021.105228.
- Donovan M, Monaghan R 2021. Impacts of grazing on ground cover, soil physical properties and soil loss via surface erosion: a novel geospatial modelling approach. Journal of Environmental Management 287: 112206. https://doi.org/10.1016/j.jenvman.2021.112206.
- Douglas G, Dymond J, McIvor I 2008. Monitoring and reporting of whole farm plans as a tool for affecting land use change. Report for Horizons Regional Council. Palmerston North, AgResearch.
- Douglas GB, McIvor IR, Manderson AK, Koolaard JP, Todd M, Braaksma S, et al. 2013. Reducing shallow landslide occurrence in pastoral hill country using wide spaced trees. Land Degradation and Development 24: 103–114.
- Douglas GB, McIvor IR, Manderson AK, Todd M, Braaksma S, Gray RAJ 2009. Effectiveness of space-planted trees for controlling soil slippage on pastoral hill country. In: Currie LD, Lindsay CL eds. Nutrient management in a rapidly changing world. Occasional Report No. 22. Palmerston North, Fertilizer and Lime Research Centre, Massey University.
- Dymond JR, Ausseil AG, Shepherd JD, Buettner L 2006. Validation of a region-wide model of landslide susceptibility in the Manawatu–Wanganui region of New Zealand. Geomorphology 74: 70–79.
- Dymond JR, Betts HD, Schierlitz CS 2010. An erosion model for evaluating regional land-use scenarios. Journal of Environmental Modelling Software 25(3): 289–298.
- Dymond JR, Davies-Colley RJ, Hughes AO, Matthaei CD 2017. Predicting improved optical water quality in rivers resulting from soil conservation actions on land. Science of the Total Environment 603: 584-592.
- Dymond J, Herzig A, Basher L, Betts HD, Marden M, Phillips CJ, et al. 2016. Development of a New Zealand SedNet model for assessment of catchment-wide soil-conservation works. Geomorphology 257: 85–93.
- Dymond JR, Shepherd JD 2004. The spatial distribution of indigenous forest and its composition in the Wellington region, New Zealand, from ETM+ satellite imagery. Remote Sensing of Environment 90: 116–125.

- Elliott AH, Semadeni-Davies AF, Shankar U, Zeldis JR, Wheeler DM, Plew DR, et al. 2016. A national-scale GIS-based system for modelling impacts of land use on water quality. Environmental Modelling & Software 86: 131–144.
- Eyles GO 1983. The distribution and severity of present soil erosion in New Zealand. New Zealand Geographer 39(1): 12–28.
- Foster GR, Meyer LD, Onstad CA 1977. A runoff erosivity factor and variable slope length exponents for soil loss estimates. Transactions of the ASAE 20(4): 683–687.
- Fransen PJB, Brownlie RK 1995. Historical slip erosion in catchments under pasture and radiata pine forest, Hawke's Bay hill country. New Zealand Journal of Forestry 40(4): 29–33.
- Fuller IC, Riedler RA, Bell R, Marden M, Glade T 2016. Landslide-driven erosion and slope-channel coupling in steep, forested terrain, Ruahine Ranges, New Zealand, 1946–2011. Catena 142: 252–268.
- Gill MA 1979. Sedimentation and useful life of reservoirs. Journal of Hydrology 44(1): 89-95.
- Hancox GT, Wright K 2005. Analysis of landsliding caused by the February 2004 rainstorms in the Wanganui–Manawatu hill country, southern North Island, New Zealand. Institute of Geological & Nuclear Sciences Science Report 2005/11. Wellington, GNS.
- Hawley JG, Dymond JR 1988. How much do trees reduce landsliding? Journal of Soil and Water Conservation 43(6): 495–498.
- Hicks DL 1989. Storm damage to bush, pasture and forest: some evidence from Cyclone Bola. DSIR Land Resources Technical Record PN2. Palmerston North, DSIR.
- Hicks DL 1990. Landslide damage to pasture, pine plantations, scrub and bush in Taranaki. DSIR Land Resources Technical Record 31. Lower Hutt, DSIR.
- Hicks DL 1991. Erosion under pasture, pine plantations, scrub and indigenous forest: a comparison from Cyclone Bola. New Zealand Forestry 36(3): 21–22.
- Hicks DM, Haddadchi A, Whitehead A, Shankar U 2019. Sediment load reductions to meet suspended and deposited sediment thresholds. NIWA Client Report 2019100CH, prepared for Ministry for the Environment.
- Hicks DM, Shankar U 2020. Sediment load reduction to meet visual clarity bottom lines. Memo prepared for Ministry for the Environment. 9 p. https://environment.govt.nz/assets/publications/Files/technical-report-6-sediment-load-reductions-to-meet-visual-clarity-bottom-lines.pdf (accessed Nov 2024).
- Hughes AO 2016. Riparian management and stream bank erosion in New Zealand. New Zealand Journal of Marine and Freshwater Research 50 (2): 277–290.
- Klik A, Haas K, Dvorackova A, Fuller IC 2015. Spatial and temporal distribution of rainfall erosivity in New Zealand. Soil Research 53: 815–825.
- Land Information New Zealand (LINZ), 2021. Waikato LiDAR 1m DEM (2021). [online] https://data.linz.govt.nz/layer/113203-waikato-lidar-1m-dem-2021/ (accessed July 2024).
- Laurenson S, Houlbrooke DJ, Beukes PC, 2016. Assessing the production and economic benefits from preventing cows grazing on wet soils in New Zealand. Journal of the Science of Food and Agriculture 96: 4584–4593.

- Leathwick J, Wilson G, Rutledge D, Wardle P, Morgan F, Johnston K, McLeod M, Kirkpatrick R 2003. Land Environments of New Zealand. Auckland, David Bateman.
- Line DE, Harman WA, Jennings GD, Thompson EJ, Osmond DL 2000. Nonpoint-source pollutant load reductions associated with livestock exclusion. Journal of Environmental Quality 29: 1882–1890.
- Manderson A, Douglas G, Mackay A, Dymond JR 2011. SLUI Outcomes project: review of the SLUI database and development of a SLUI outcomes reporting framework. Report prepared for Horizons Regional Council by AgResearch.
- Marden M 2012. Effectiveness of reforestation in erosion mitigation and implications for future sediment yields, East Coast catchments, New Zealand: a review. New Zealand Geographer 68: 24–35.
- Marden M, Phillips CJ 2013. Survival and growth of poplar and willow pole plantings on East Coast hill country. Landcare Research Contract Report LC1622, prepared for Plant and Food Research.
- Marden M, Phillips CJ, Rowan D 1991. Declining soil loss with increasing age of plantation forests in the Uawa catchment, East Coast region. In: Henriques PR ed. Proceedings, International Conference on Sustainable Land Management, Napier, Hawke's Bay, New Zealand, 17–23 November 1991. Pp. 358–361.
- Marden M, Rowan D 1993. Protective value of vegetation on Tertiary terrain before and during Cyclone Bola, East Coast, North Island, New Zealand. New Zealand Journal of Forestry Science 23: 255–263.
- McCool DK, Foster GR, Mutchler CK, Meyer LD 1989. Revised slope length factor for the universal soil loss equation. Transactions of the ASAE 32(5): 1571–1576.
- McIvor I, Clarke K, Douglas G 2015. Effectiveness of conservation trees in reducing erosion following a storm event. In: Currie LD, Burkitt LL eds. Proceedings, 28th Annual Fertiliser and Lime Research Centre Workshop 'Moving farm systems to improved attenuation'. Occasional Report 28. Palmerston North, Fertiliser and Lime Research Centre.
- McIvor I, Douglas G, Dymond JR, Eyles G, Marden M 2011. Pastoral hillslope erosion in New Zealand and the role of poplar and willow trees in its reduction. In: Godone D, Stanchi eds. Soil erosion issues in agriculture. London, IntechOpen Pp. 257–278. http://www.intechopen.com/articles/show/title/pastoral-hill-slope-erosion-in-new-zealand-and-the-role-of-poplar-and-willow-trees-in-its-reduction.
- McKergow LA, Tanner CC, Monaghan RM, Anderson G 2007. Stocktake of diffuse pollution attenuation tools for New Zealand pastoral farming systems. NIWA Client Report HAM2007-161 prepared for Pastoral 21 Research Consortium. Hamilton, National Institute of Water and Atmospheric Research.
- McKergow LA, Weaver DM, Prosser IP, Grayson RB, Reed AE 2003. Before and after riparian management: sediment and nutrient exports from a small agricultural catchment, Western Australia. Journal of Hydrology 270(3-4): 253–72.
- Meals DW, Hopkins RB 2002. Phosphorus reductions following riparian restoration in two agricultural watersheds in Vermont, USA. Water Science and Technology 45(9): 51–60.

- Ministry for the Environment (MfE) 2022. Guidance for implementing the NPS-FM sediment requirements. Wellington, Ministry for the Environment.
- Ministry for the Environment 2020. National Policy Statement for Freshwater Management 2020. Wellington, Ministry for the Environment.
- Monaghan RM, Quinn J 2010. Appendix 9: Farms. National Institute of Water and Atmospheric Research (NIWA), Waikato River Independent Scoping Study. Hamilton, NIWA.
- Nearing MA, Yin S, Borrelli P, Polyakov VO 2017. Rainfall erosivity: an historical review. Catena 157: 357–362.
- Neverman A, Smith HG, Herzig A, Basher LR 2021. Modelling baseline suspended sediment loads and load reductions required to achieve draft freshwater objectives for Southland. Manaaki Whenua Landcare Research Contract Report LC3749, prepared for Environment Southland.
- Newsome PFJ, Wilde RH, Willoughby EJ 2008. Land Resource Information System spatial data layers: data dictionary. Palmerston North, Landcare Research. http://digitallibrary.landcareresearch.co.nz/cdm/ref/collection/p20022coll14/id/67.
- Norris M, Jones H, Kimberley M, Borman D 2020. Riparian characteristics of pastoral waterways in the Waikato region, 2002-2017. Waikato Regional Council Technical Report 2020/12. Hamilton, Waikato Regional Council.
- Norris M, Norris T, 2021. Catchment riparian characteristics survey of Matahuru catchment (2021). Waikato Regional Council Internal Series 2021/05. Hamilton, Waikato Regional Council.
- Norris T, 2022. Riparian characteristics survey of the Kaniwhaniwha catchment (2022). Waikato Regional Council Internal Series 2023/18. Hamilton, Waikato Regional Council.
- Norris T, Morgan E, Piggott E, 2023. Riparian Characteristics Survey of the Moakurarua Catchment (2023). Waikato Regional Council Internal Series 2023/07. Hamilton, Waikato Regional Council.
- Owens LB, Edwards WM, Van Keuren RW 1996. Sediment losses from a pastured watershed before and after fencing. Journal of Soil and Water Conservation 51(1): 90–94.
- Page MJ, Reid LM, Lynn IH 1999. Sediment production from Cyclone Bola landslides, Waipaoa catchment. Journal of Hydrology (NZ) 38: 289–308.
- Page MJ, Trustrum NA, Dymond JR 1994. Sediment budget to assess the geomorphic effect of a cyclonic storm, New Zealand. Geomorphology 9(3): 169–188.
- Pain CF, Stephens PR 1990. Storm damage assessment using digitised aerial photographs: Eltham, New Zealand, 24–25 February 1986. New Zealand Geographer 46: 21–25.
- Palmer D, Dymond J, Basher L 2013. Assessing erosion in the Waipa catchment using the New Zealand Empirical Erosion Model (NZeem®), Highly Erodible Land (HEL), and SedNetNZ models. Landcare Research Contract Report LC1685, prepared for Waikato Regional Council.
- Palmer D, Dymond J, Herzig A, Betts H, Marden M, Basher L 2015. SedNetNZ modelling of the Waikato catchment. Landcare Research Contract Report LC2428, prepared for Waikato Regional Council.
- Phillips C, Basher L, Spiekermann R 2020. Biophysical performance of erosion and sediment control techniques in New Zealand: a review. Landcare Research Contract Report LC3761, prepared for the Smarter Targeting of Erosion Control (STEC) MBIE research programme.

- Phillips C, Betts, H, Smith HG, Tsyplenkov A 2024. Exploring the post-harvest 'window of vulnerability' to landslides in New Zealand steepland plantation forests. Ecological Engineering 206: 10N7300. https://doi.org/10.1016/j.ecoleng.2024.107300
- Phillips C, Hales T, Smith H, Basher L 2021. Shallow landslides and vegetation at the catchment scale: a perspective. Ecological Engineering173: 106436. https://doi.org/10.1016/j.ecoleng.2021.106436.
- Phillips C, Marden M, Basher LR 2018. Geomorphology and forest management in New Zealand's erodible steeplands: an overview. Geomorphology 307: 107–121.
- Phillips CJ, Marden M, Pearce A 1990. Effectiveness of reforestation in prevention and control of landsliding during large cyclonic storms. Proceedings of the 19th World IUFRO Congress (Division 1, Vol. 1), Montreal, Canada, August 1990. Pp. 340–350.
- Reichenbach P, Rossi M, Malamud BD, Mihir M, Guzzetti F 2018. A review of statistically-based landslide susceptibility models. Earth-Science Reviews 180: 60–91.
- Reid LM, Page MJ 2002. Magnitude and frequency of landsliding in a large New Zealand catchment. Geomorphology 49: 71–88.
- Renard KG 1997. Predicting soil erosion by water: a guide to conservation planning with the Revised Universal Soil Loss Equation (RUSLE). Washington, DC, United States Government Printing.
- Rosewell CJ, Loch RJ 2002. Estimation of the RUSLE soil erodibility factor. In: McKenzie N, Coughlan K, Cresswell H eds. Soil physical measurement and interpretation for land evaluation. Melbourne, Australia, CSIRO Publishing.
- Semadeni-Davies A, Elliott S 2016. Modelling the effect of stock exclusion on *E. coli* in rivers and streams: national application. Technical Paper No. 2017/10, prepared for Ministry for Primary Industries by NIWA.
- Smith HG, Herzig A, Dymond JR, Basher LR 2019. Application of a revised SedNetNZ model to the Oreti and Aparima catchments, Southland. Manaaki Whenua Landcare Research Contract Report LC3507, prepared for Our Land & Water National Science Challenge.
- Smith HG, Neverman A, Betts H, Herzig A 2024. Improving understanding and management of erosion with LiDAR. Landcare Research Contract Report LC4466, prepared for Hawke's Bay Regional Council.
- Smith HG, Neverman AJ, Betts H, Spiekermann R 2023. The influence of spatial patterns in rainfall on shallow landslides. Geomorphology 437: 108795. https://doi.org/10.1016/j.geomorph.2023.108795
- Smith HG, Spiekermann R, Betts H, Neverman AJ 2021. Comparing methods of landslide data acquisition and susceptibility modelling: Examples from New Zealand. Geomorphology 381: 107660. https://doi.org/10.1016/j.geomorph.2021.107660
- Smith HG, Spiekermann R, Dymond J, Basher L 2019. Predicting spatial patterns in riverbank erosion for catchment sediment budgets. New Zealand Journal of Marine and Freshwater Research 53(3): 338–362.
- Smith HG, Spiekermann R, Betts H, Neverman AJ 2020. Application of a revised bank erosion model to update SedNetNZ results for Hawke's Bay. Manaaki Whenua Landcare Research Contract Report LC3740, prepared for Hawke's Bay Regional Council.

- Spiekermann RI, McColl S, Fuller I, Dymond J, Burkitt L, Smith HG 2021. Quantifying the influence of individual trees on slope stability at landscape scale. Journal of Environmental Management 286: 112194. https://doi.org/10.1016/j.jenvman.2021.112194
- Trimble SW 1994. Erosional effects of cattle on streambanks in Tennessee, U.S.A. Earth Surface Processes and Landforms 19(5): 451–464.
- Vale SS, Smith HG, Neverman A, Herzig A 2021. Application of SedNetNZ with land management and climate change scenarios and temporal disaggregation in the Bay of Plenty Region.

 Manaaki Whenua Landcare Research Contract Report LC4002, prepared for Bay of Plenty Regional Council.
- Vale S, Smith H 2024. Application of SedNetNZ in the Waikato region to support NPS-FM 2020 implementation. Manaaki Whenua Landcare Research Contract Report LC4432, prepared for Waikato Regional Council.
- Vercruysse K, Grabowski RC, Rickson RJ 2017. Suspended sediment transport dynamics in rivers: Multi-scale drivers of temporal variation. Earth-Science Reviews 166: 38–52. https://doi.org/10.1016/j.earscirev.2016.12.016
- Waikato Regional Council (WRC) 2020. Proposed Waikato Regional Plan Change 1: Waikato and Waipā River Catchments (Decisions Version). Waikato Regional Council Policy Series 2020/02. www.waikatoregion.govt.nz. (accessed September 2024).
- Wang G, Gertner G, Liu X, Anderson A 2001. Uncertainty assessment of soil erodibility factor for revised universal soil loss equation. Catena 46(1): 1–14.
- Whitehead AL, Booker DJ 2020. NZ river maps: an interactive online tool for mapping predicted freshwater variables across New Zealand. Christchurch, NIWA. https://shiny.niwa.co.nz/nzrivermaps/
- Williamson R, Smith C, Cooper A 1996. Watershed riparian management and its benefits to a eutrophic lake. Journal of Water Resources Planning and Management 122: 24–32.
- Wischmeier WH, Johnson C, Cross B 1971. Soil erodibility nomograph for farmland and construction sites. Journal of Soil and Water Conservation 26(5): 189–193.
- Wischmeier WH, Smith DD 1978. Predicting rainfall erosion losses—a guide to conservation planning, agriculture handbook. Indiana, USA, United States Department of Agriculture.
- Woods R, Hendrikx J, Henderson R, Tait A 2006. Estimating mean flow of New Zealand rivers. Journal of Hydrology (New Zealand) 45(2): 95–109.
- Yang X, Gray J, Chapman G, Zhu Q, Tulau M, McInnes-Clarke S 2018. Digital mapping of soil erodibility for water erosion in New South Wales, Australia. Soil Research 56(2): 158–170.
- Zhang X, Liu X, Zhang M, Dahlgren RA, Eitzel M 2010. A Review of vegetated buffers and a metaanalysis of their mitigation efficacy in reducing nonpoint source pollution. Journal of Environmental Quality 39(1): 76–84.

Appendix 1

Table A1.1. Summary of layers associated with the LiDAR-based version of SedNetNZ supplied with the present report

Folder name	Layer name	Description
Watershed_layers	Kaniwhaniwha_streamlines_v1.0.shp Karapiro_streamlines_v1.0.shp Matahuru_streamlines_v1.0.shp Moakurarua_streamlines_v1.0.shp	Digital streamlines representing the drainage network with a 5-ha upstream area threshold for channel initiation. CATCHMENT – CEM catchment name HydroID – unique identifier of each subwatershed NextDownID – HydroID of the next downstream subwatershed LengthKM – streamline length in km StrOrd – Stream order (1 – 8)
Watershed_layers	Kaniwhaniwha_subwatershed_v1.0.shp Karapiro_subwatershed_v1.0.shp Matahuru_subwatershed_v1.0.shp Moakurarua_subwatershed_v1.0.shp	Subwatersheds draining to segments within the digital stream network. CATCHMENT – CEM catchment name HydroID – unique identifier of each subwatershed NextDownID – HydroID of the next downstream subwatershed AreaKM2 – subwatershed area in km²
Modelled_layers	Kaniwhaniwha_C2023_LiDAR_SedNetNZ_v1.0.shp Karapiro_C2023_LiDAR_SedNetNZ_v1.0.shp Matahuru_C2023_LiDAR_SedNetNZ_v1.0.shp Moakurarua_C2023_LiDAR_SedNetNZ_v1.0.shp	LiDAR-based SedNetNZ suspended sediment budget for each subwatershed in the CEM catchments based on 2018 land cover from LCDB v5.0 and existing soil conservation works (C2023). The shapefile contains the following fields: • HydroID – unique identifier of each subwatershed • NextDownID – HydroID of the next downstream subwatershed • AreaKM2 – subwatershed area in km² • LandsIYId – mean annual suspended sediment yield (t km² yr¹) from shallow landslides delivered to the stream segment within a subwatershed • SurfaceYId – mean annual suspended sediment yield (t km² yr¹) from surface erosion delivered to the stream segment within a subwatershed

Folder name	Layer name	Description
Modelled_layers (Cont.)	Kaniwhaniwha_C2023_LiDAR_SedNetNZ_v1.0.shp	 EarthflYld – mean annual suspended sediment yield (t km⁻² yr⁻¹) from earthflow erosion delivered to the stream segment within a subwatershed
	Karapiro_C2023_LiDAR_SedNetNZ_v1.0.shp Matahuru_C2023_LiDAR_SedNetNZ_v1.0.shp	 GullyYld – mean annual suspended sediment yield (t km⁻² yr⁻¹) from gully erosion delivered to the stream segment within a subwatershed
	Moakurarua_C2023_LiDAR_SedNetNZ_v1.0.shp	 RivBankYld – mean annual suspended sediment yield (t km⁻² yr⁻¹) from net riverbank erosion delivered to the stream segment within a subwatershed
	(Cont.)	 TotalSedYld – total mean annual suspended sediment yield (t km⁻² yr⁻¹) delivered to the stream segment from all erosion processes present within a subwatershed
		 AccNetLoad – net suspended sediment load that accumulates downstream while accounting for losses of sediment into long-term storage in lakes and on floodplains (t yr⁻¹)
Modelled_layers	Kaniwhaniwha_XX_SedYld_LiDAR_SedNetNZ_v1.0.shp Karapiro_XX_SedYld_LiDAR_SedNetNZ_v1.0.shp Matahuru_XX_SedYld_LiDAR_SedNetNZ_v1.0.shp	LiDAR-based SedNetNZ total mean annual suspended sediment yield (t km ⁻² yr ⁻¹) for each subwatershed in the CEM catchments based on the erosion mitigation scenarios (M1 and M2). The shapefile contains the following fields:
	Moakurarua_XX_SedYld_LiDAR_SedNetNZ_v1.0.shp	HydroID – unique identifier of each subwatershed
		AreaKM2 – subwatershed area in km²
	XX = • M1 or M2	 XX_XXXX – total mean annual suspended sediment yield (t km⁻² yr⁻¹) delivered to the stream segment from all erosion processes present within a subwatershed for the respective scenario
		 M1_20_yld, M1_30_yld, M1_40_yld, M1_50_yld, M1_100_yld,
		M1_aff_yld, M1_spa_yld, M1_rip_yld
		 M2_20_yld, M2_30_yld, M2_40_yld, M2_50_yld, M2_100_yld,
		M2_aff_yld, M2_spa_yld, M2_rip_yld
		 Rank_M1 – ranked subwatershed for size of load reduction for M1 scenario
		 Rank_M2 – ranked subwatershed for size of load reduction for M2 scenario

Folder name	Layer name	Description
Modelled_layers	Kaniwhaniwha_XX_NetLd_LiDAR_SedNetNZ_v1.0.shp Karapiro_XX_NetLd_LiDAR_SedNetNZ_v1.0.shp Matahuru_XX_NetLd_LiDAR_SedNetNZ_v1.0.shp	LiDAR-based SedNetNZ mean annual net suspended sediment load (t yr ⁻¹) that accumulates downstream for each subwatershed in the CEM catchments based on the erosion mitigation scenarios (M1 and M2).
	Moakurarua_XX_NetLd_LiDAR_SedNetNZ_v1.0.shp	The shapefile contains the following fields:
	XX =	HydroID – unique identifier of each subwatershed
	• M1 or M2	AreaKM2 – subwatershed area in km²
		 XX_XX_XXX – mean annual net suspended sediment load that accumulates downstream while accounting for losses of sediment into long-term storage in lakes and on floodplain for each respective scenario (t yr⁻¹)
		 M1_20_nld, M1_30_nld, M1_40_nld, M1_50_nld, M1_100_nld, M1_aff_nld, M1_spa_nld, M1_rip_nld
		 M2_20_nld, M2_30_nld, M2_40_nld, M2_50_nld, M2_100_nld, M2_aff_nld, M2_spa_nld, M2_rip_nld
		Rank_M1 – ranked subwatershed for size of load reduction for M1 scenario
		Rank_M2 – ranked subwatershed for size of load reduction for M2 scenario
Shallow_landslide	Kaniwhaniwha_XXX_ShallowLandslideErosion_v1.0.tif Karapiro_XXX_ShallowLandslideErosion_v1.0.tif Matahuru_XXX_ShallowLandslideErosion_v1.0.tif Moakurarua_XXX_ShallowLandslideErosion_v1.0.tif	Raster layer (5 m grid) of mean annual suspended sediment yield (t km ⁻² yr ⁻¹) from rainfall-induced shallow landslide erosion delivered to the stream network for contemporary baseline (C2023) and full implementation of each erosion mitigation scenario (M1 and M2).
	XXX =	For sediment budgeting, the sediment yield from shallow landslide erosion is derived by
	• C2023	averaging across all pixels within a subwatershed.
	• M1	
	• M2	

Folder name	Layer name	Description
Surface_erosion	Kaniwhaniwha_XXX_SurfaceErosion_v1.0.tif Karapiro_XXX_SurfaceErosion_v1.0.tif Matahuru_XXX_SurfaceErosion_v1.0.tif	Raster layer (5 m grid) of mean annual suspended sediment yield (t km ⁻² yr ⁻¹) from surface erosion delivered to the stream for contemporary baseline (C2023) and full implementation of each erosion mitigation scenario (M1 and M2).
	Moakurarua_XXX_SurfaceErosion_v1.0.tif XXX = • C2023 • M1 • M2	At the pixel scale, very high sediment yields from surface erosion occur when expressed per km² in some cases due to the combination of high erosion rates and the small pixel size (1 pixel = 25 m²). For sediment budgeting, the sediment yield from surficial erosion is derived by averaging across all pixels within a subwatershed. The sediment yields account for sediment trapping by riparian buffers, which is determined for each subwatershed and applied across all pixels within the subwatershed.
Visual_clarity	SOE_C2023_proportional_reductions_v1.0.shp SOE_M1_proportional_reductions_v1.0.shp SOE_M2_proportional_reductions_v1.0.shp	Modelled reductions in suspended sediment loads for contemporary baseline and erosion mitigation scenarios required to achieve each NPSFM (2020) attribute band and NBL for suspended fine sediment. Provided as proportional reductions and load reductions (t yr ⁻¹)
	SOE_C2023_proportional_reductions_v1.0.shp	Site_name – Name of SOE monitoring site
	SOE_M1_sediment_load_reductions_v1.0.shp	Site_ID – Site ID of SOE monitoring site
	SOE_M2_sediment_load_reductions_v1.0.shp	HydroID – unique identifier of each subwatershed
		 SedClass – Suspended sediment class (1-4) based on REC segments (Hicks & Shankar (2020))
		 CLAR – Estimated baseline visual clarity for each SOE site (based on data provided)
		 base_stat – Estimated base state (based on data provided)
		 NBL_XX, B_XX, A_XX - Proportional reductions to achieve NPS-FM (2020) for band A, B and NBL (C). Suffixes refer to respective scenarios.
		• C2023
		 M1_20, M1_30, M1_40, M1_50, M1_100, M1_aff, M1_spa, M1_rip
		 M2_20, M2_30, M2_40, M2_50, M2_100, M2_aff, M2_spa, M2_rip